OCEANOGRAPHY

Unexpected fish and squid in the central Arctic deep scattering layer

Pauline Snoeijs-Leijonmalm[1]*, Hauke Flores[2], Serdar Sakinan[3], Nicole Hildebrandt[2],
Anders Svenson[4], Giulia Castellani[2], Kim Vane[2], Felix C. Mark[2], Céline Heuzé[5],
Sandra Tippenhauer[2], Barbara Niehoff[2], Joakim Hjelm[4], Jonas Hentati Sundberg[4],
Fokje L. Schaafsma[3], Ronny Engelmann[6], The EFICA-MOSAiC Team†

The retreating ice cover of the Central Arctic Ocean (CAO) fuels speculations on future fisheries. However, very little is known about the existence of harvestable fish stocks in this 3.3 million–square kilometer ecosystem around the North Pole. Crossing the Eurasian Basin, we documented an uninterrupted 3170-kilometer-long deep scattering layer (DSL) with zooplankton and small fish in the Atlantic water layer at 100- to 500-meter depth. Diel vertical migration of this central Arctic DSL was lacking most of the year when daily light variation was absent. Unexpectedly, the DSL also contained low abundances of Atlantic cod, along with lanternfish, armhook squid, and Arctic endemic ice cod. The Atlantic cod originated from Norwegian spawning grounds and had lived in Arctic water temperature for up to 6 years. The potential fish abundance was far below commercially sustainable levels and is expected to remain so because of the low productivity of the CAO.

INTRODUCTION

The Arctic region is the most rapidly warming part of Earth (1). As a consequence, the marine ecosystem around the North Pole, the Central Arctic Ocean (CAO), is in fast transition from a permanently to a seasonally ice-covered ocean (2). This implies a huge environmental modification of Earth's northernmost ecosystem, which consists of deep intercontinental basins and submarine ridges covering an area of 3.3 million km^2 (Fig. 1A) (3). Increasing accessibility to the CAO in the near future is expected to affect ecological and social dynamics, including the possible onset of commercial fisheries. However, the lack of data on pelagic fish stocks beneath the sea ice cover impedes any assessment of the sustainability of potential future fisheries in the CAO (4–6).

Since mesopelagic nekton (actively swimming organisms) plays a key role in controlling carbon flux and nutrient dynamics in other marine ecosystems (7), closing this knowledge gap for the CAO is crucial for predictions of future ecological change, as well as for conservation and resource management. Traditional fishery assessments are based on trawling and hydroacoustics in combination. While trawled nets cannot be applied in the CAO today due to its up to ca. 3-m-thick ice cover, acoustic data collection is also problematic because hydroacoustic backscatter from organisms is distorted by the noise from icebreaking. Thus, as a result of uncompromising logistical difficulties in studying nekton and macrozooplankton, marine biological studies in the water column of the CAO have focused on lower trophic levels, from microbes to mesozooplankton.

The possibility of future resource exploitation in the high seas portion of the CAO (Fig. 1A), i.e., international waters outside national jurisdictions, is debated at national and international political levels. Usually, exploitation of newly accessible natural resources tends to precede scientific research and management measures, and internationally shared fish stocks in high seas are especially prone to overexploitation (8). However, taking a precautionary approach, nine countries and the European Union negotiated the *Agreement to Prevent Unregulated High Seas Fisheries in the Central Arctic Ocean* (www.fao.org/faolex/results/details/en/c/LEX-FAOC199323) that entered into force on 25 June 2021. This agreement prevents any commercial fishing for at least 16 years to come and puts "science first," warranting scientific assessments of the status and distribution of possible fish stocks in the CAO and the ecosystem supporting them (9).

Horizontal zones with living organisms (zooplankton and nekton), so-called "deep scattering layers" (DSLs) detected as acoustic backscatter by an echosounder, are widespread in the World's oceans (7, 10) and could be driven to the poles by climate change (11). Animals causing DSLs typically perform diel vertical migration (DVM) in response to diurnal changes in sunlight to avoid visual predators during the day. DVM is a fundamental component of the biological carbon pump that transports carbon from the atmosphere and land runoff to the deep ocean (7, 10). Thus, oceans without a biological carbon pump would result in much higher carbon dioxide levels in Earth's atmosphere than we have today. The first observations of the existence of a central Arctic DSL were made from the Swedish icebreaker *Oden* in summer 2016 (12). This DSL was situated at mesopelagic depths (300 to 600 m) in the Atlantic water layer of the CAO in summer and had its highest density around the North Pole. The 13 hydroacoustic stations studied were widespread in the CAO (Canada, Makarov, Amundsen, and Nansen Basins), but hydroacoustic measurements were limited to, on average, only 6 hours per station, and no fish were sampled. The central Arctic DSL could (partly) be a continuation of the mesopelagic DSL reported from the area immediately south of the CAO up to 82.1°N (13–15) and across the entire Fram Strait at the Atlantic gateway to the Arctic Ocean (16).

[1]Department of Ecology, Environment and Plant Sciences, Stockholm University, 10691 Stockholm, Sweden. [2]Alfred-Wegener-Institut, Helmholtz-Zentrum für Polar- und Meeresforschung, 27570 Bremerhaven, Germany. [3]Wageningen Marine Research, 1970 AB IJmuiden, Netherlands. [4]Department of Aquatic Resources, Swedish University of Agricultural Sciences, 45330 Lysekil, Sweden. [5]Department of Earth Sciences, University of Gothenburg, 40530 Gothenburg, Sweden. [6]Leibniz Institute for Tropospheric Research, 04318 Leipzig, Germany.
*Corresponding author. Email: pauline.snoeijs-leijonmalm@su.se
†See the Supplementary Materials.
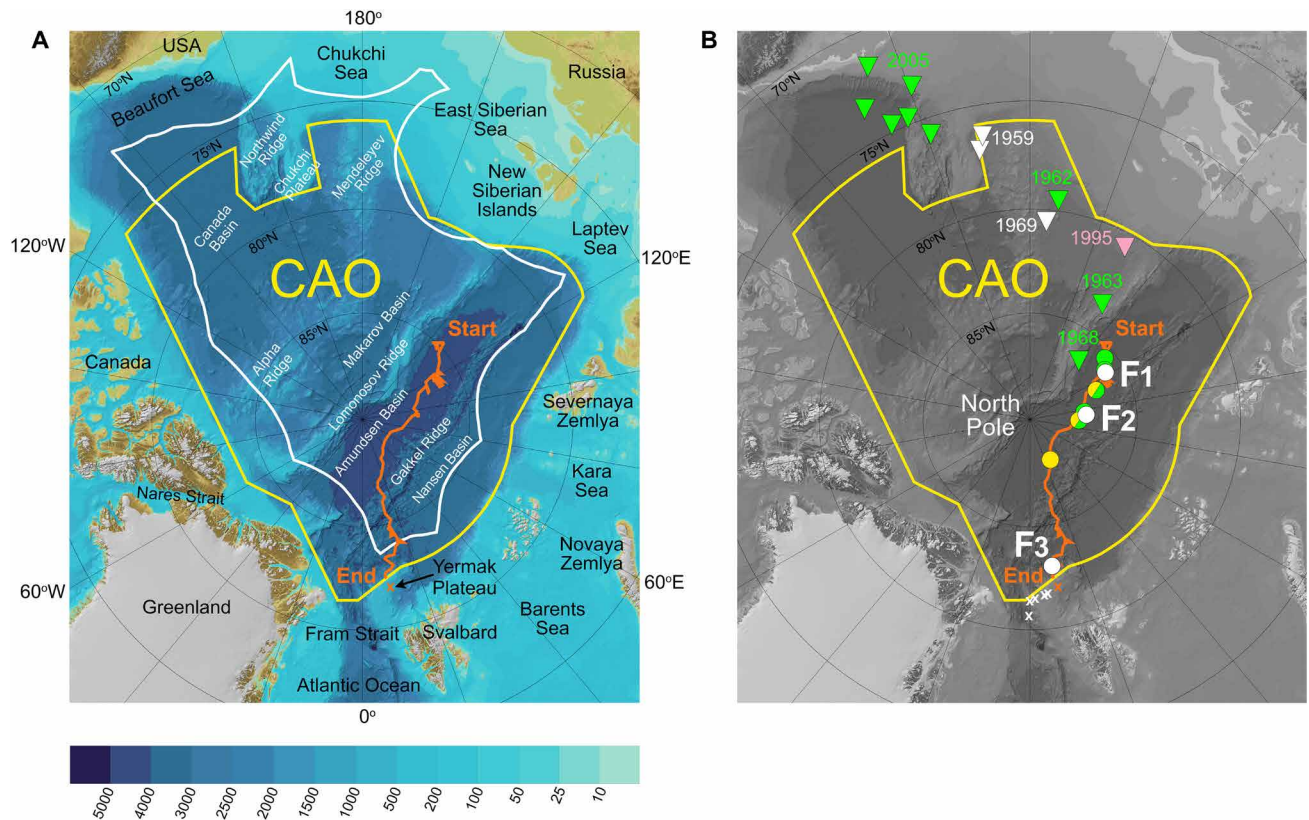
Fig. 1. Maps of the CAO. (**A**) Geographical map showing the 3170-km-long track during legs 1 to 3 of the MOSAiC expedition (orange line). The starting point for the acoustic measurements was at 85.1°N, 136.5°E (1 October 2019), and the end point was at 82.4°N, 8.3°E (27 May 2020). The yellow line represents the border of the CAO marine ecosystem as defined by the Arctic Council (*3*). The white line represents the border of the high seas portion of the Arctic Ocean, i.e., the area outside the Exclusive Economic Zones of the five coastal states. The background map was extracted from the International Bathymetric Chart of the Arctic Ocean, version 3.0 (*70*); bathymetric colors indicate meters below mean sea level. (**B**) Map of the CAO, showing the locations where fish were sampled (white circles, areas F1 to F3) or where fish and armhook squid were recorded on video (yellow circle, only fish; mixed yellow and green circle, both fish and squid; green circle, only squid), along the track [orange line, cf. (A)]. Station X, additional acoustic data collection (orange X) and additional fish sampled (white X) during leg 4 of the MOSAiC expedition at the Yermak Plateau south of the track. Triangles show all previously published records of pelagic nekton in the CAO (i.e., excluding sympagic polar cod at the sea surface and benthic species) and the recording year. The white triangles show all previously published records of ice cod in the upper 25-m water layer (*18*, *20*). The pink and green triangles inside the CAO show all records of juvenile and adult armhook squid, respectively (*23*, *24*, *52*). The green triangles outside the CAO show video records of armhook squid in the Beaufort Sea (*50*).

Besides anecdotal reports of unidentified pelagic fish from submarine windows in the 1950s and 1960s (*17*), fish observations in the CAO have been restricted to the sympagic (ice-associated) and benthic habitats. A well-known phenomenon is the occurrence of sympagic juvenile polar cod (*Boreogadus saida*) at the ocean surface (*18*, *19*), while ice cod (*Arctogadus glacialis*) has rarely been reported from the same habitat down to 25 m of depth (*18*), as well as by seismic blasts set off at 15 m of depth on the edge of the CAO near the Chukchi Plateau (Fig. 1B) (*20*). There is some confusion about the vernacular names for these two Arctic endemic gadoids. This paper follows the translation of the scientific name into the vernacular name, i.e., "ice cod" for *A. glacialis*, and "polar cod" for *B. saida*, since "Arctic cod" is commonly used for Atlantic cod (*Gadus morhua*) belonging to the Arcto-Norwegian cod stock.

Some other commercial species inhabiting Arctic continental slope areas, such as Greenland halibut (*Reinhardtius hippoglossoides*) and beaked redfish (*Sebastes mentella*), are considered candidates for moving northward to the deep central Arctic basins with further climate change (*6*, *17*). However, the probability of fish stocks to establish themselves in the CAO depends on factors such as food availability and possibilities for successful reproduction and recruitment of juveniles, i.e., factors that at present are still unexplored for the CAO (*21*, *22*). Fourteen other fish species reported from the CAO are noncommercial species living in and on muddy bottoms such as snailfishes (Liparidae) and eelpouts (Zoarcidae) (*6*). With respect to cephalopod nekton, only five individuals of the Boreo-Atlantic species armhook squid (*Gonatus fabricii*) have so far been reported from shallower water above ridges in the CAO, but not from the deep basins (Fig. 1B) (*23*, *24*).

The international MOSAiC expedition (https://mosaic-expedition.org) with the German icebreaker Research Vessel *Polarstern* (https://jlsrf.org/index.php/lsf/article/view/163/pdf_1) in 2019–2020 provided a unique possibility to collect continuous data over 8 months along a 3170-km-long track crossing the Eurasian Basin of the CAO (Fig. 1). Since this was a drift expedition with the icebreaker moored to an ice floe, acoustic signals were not disturbed by icebreaking. We applied three field approaches to studying the mesopelagic nekton along this track: hydroacoustics, video recording, and stationary

fish sampling. With this data collection, we aimed to seize the extent and the horizontal and vertical variability of the central Arctic DSL across the Eurasian Basin and to assess the distribution of fish and squid beneath the permanent pack ice of the CAO.

## RESULTS

Hydroacoustic observations

Along the 8-month track of MOSAiC legs 1 to 3 (Fig. 1), we observed a weak but consistent DSL at 100- to 500-m depth (Fig. 2) using an analytical threshold of −65 dB. The ship was continuously drifting with the sea ice, except during the last 10 days of the track when it was steaming to Svalbard. The backscatter from the DSL depicted acoustic tracks of individual targets with a target strength (TS) of −45 to −50 dB at 38 kHz, but in area F1 (Fig. 1B), echoes from larger objects (TS around −40 dB) were detected at an approximate rate of two objects passing under the ship per hour. These larger objects mainly occurred in the lower part of the DSL. The density of the DSL varied along the track (fig. S1). On the Siberian side of the Amundsen Basin, the daily mean nautical area scattering coefficient (s_A) ± SD at 38 kHz was 1.19 ± 2.05 m^2 nautical mile^{-2} from 1 October 2019 to 22 February 2020 (n = 144 days). This is 18 times higher than that on the Fram Strait side of the Amundsen and Nansen Basins (0.07 ± 0.10 m^2 nautical mile^{-2}) between 23 February and 14 May (n = 82 days). We trust that the difference in s_A between the two areas was not caused by an effect of water temperature on echosounder gain since the temperature difference between the two areas was negligible: from 1 October 2019 to 22 February 2020 [46 conductivity, temperature, and depth (CTD) casts], mean temperature ± SD = −0.8° ± 1.0°C at 0- to 200-m depth and

+1.2° ± 0.1°C at 200- to 500-m depth; from 23 February to 24 May 2020 (14 CTD casts), −1.0° ± 1.0°C at 0 to 200 m and +1.2° ± 0.3°C at 200 to 500 m. The transition between the two areas was characterized by an abrupt decrease in s_A values near 88.6°N, 64.5°E. In the end of May, when the MOSAiC ice floe approached the inflow region of Atlantic water to the Arctic Basin near 83.3°N, 9.3°E, the s_A suddenly rose by a factor of >1000 to values around 100 m^2 nautical mile^{-2}. The density of the DSL in the CAO (Fig. 3, A and B), including that in the Atlantic inflow region (Fig. 3C), was much lower than that on the continental shelf as illustrated by hydroacoustic data from one station on the Yermak Plateau south of the studied track (station X; Figs. 1 and 3D).

The highest s_A values were associated with water temperature above 0°C and salinity above 34 (Fig. 4), confirming that the DSL was located in the Atlantic water layer. We found two patterns in the vertical distribution of the DSL: (i) A distinct stable difference in DSL depth between the polar night when the sun never rises and the polar day when the sun never sets. The DSL was in the upper part of the Atlantic water layer (100 to 250 m) in the total darkness of the polar night between October and March, and it was in the lower part of the Atlantic water layer (300 to 500 m) in the constant light of the polar day in April to May (Fig. 2). Neither during the polar night nor during the polar day, there was any sign of DVM. (ii) A clear manifestation of DVM in the two brief (ca. 3 weeks long) twilight periods between the two high Arctic seasons with variation in sunlight within 1 day (in October and March) (Fig. 5).

Fish sampled in the DSL

We deployed 35 longlines and >300 fishing rods with three different hook sizes and two different baits (shrimp and squid) between
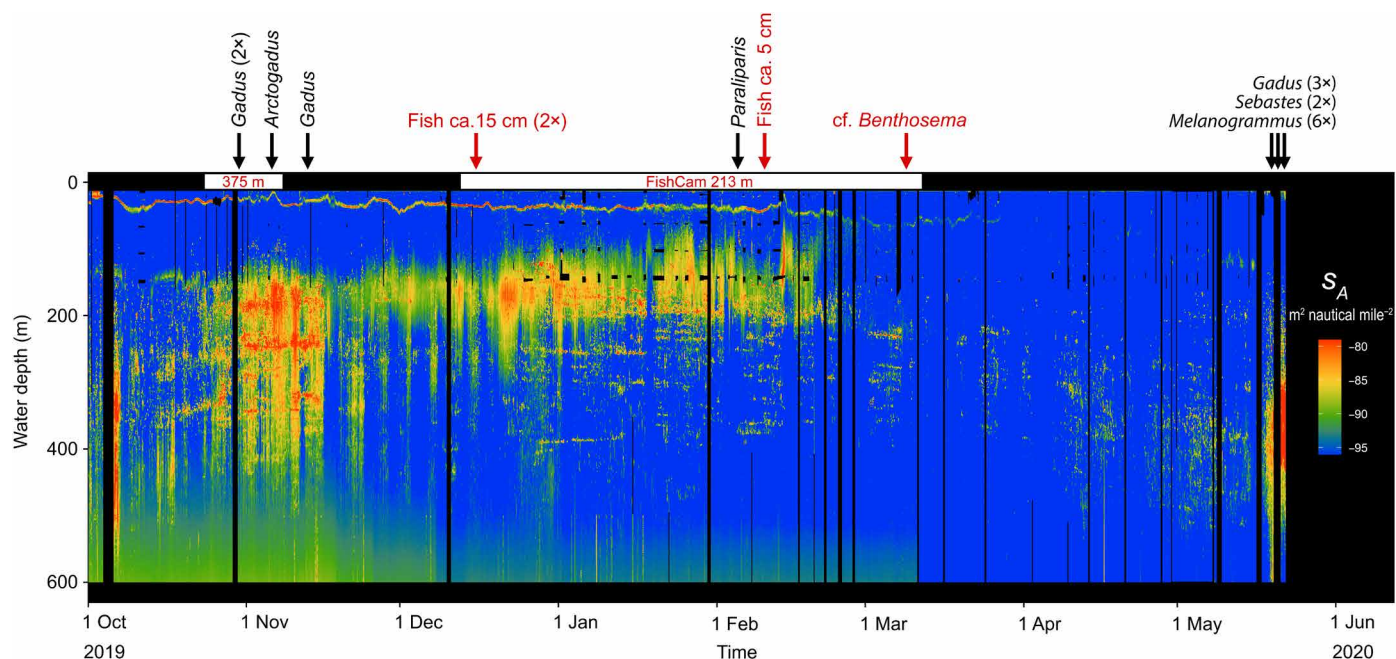
Fig. 2. The central Arctic DSL and fish records along the track of MOSAiC legs 1 to 3 (data S1). The graph shows the vertical distribution of the nautical area scattering coefficient (s_A) in the water column at 11 to 600 m of depth between the starting point of the track (1 October 2019) and its end point (27 May 2020). Black vertical lines represent short periods with no acoustic data collection. The arrows denote the time when fish was sampled in the DSL (black arrows) or observed on video recordings with the FishCam (red arrows). The FishCam was deployed at 375 ± 1 m of depth from 23 October to 7 November 2019 and at 213 ± 2 m of depth between 12 December 2019 and 11 March 2020. During other times along the track, the sea ice was too dynamic for deployment of the FishCam.
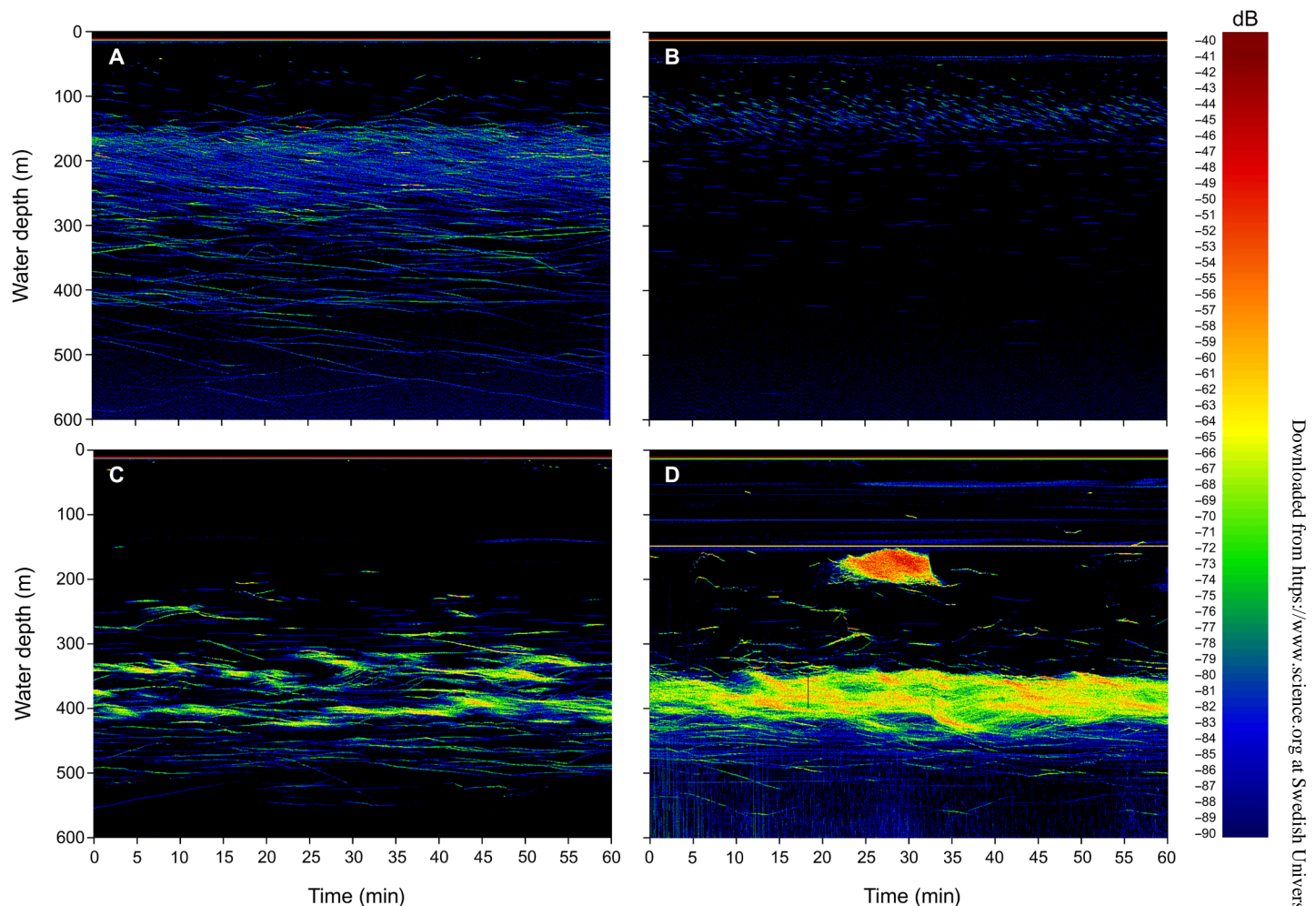
Fig. 3. Comparison of the density the central Arctic DSL in different regions along the track of MOSAiC legs 1 to 3. All four echograms include 1 hour of recording the nautical area scattering coefficient (s_A) at 11 to 600 m of depth at 38 kHz. A red color (−50 to −40 dB) indicates larger (fish-sized) organisms or smaller organisms grouped together, and object size decreases from red via orange, yellow, and green to blue. (**A**) Area F1 in the central Amundsen Basin, 5 November to 6 November 2019, 23:47 to 00:46 hours, 85.9°N, 117.9°E, showing a DSL at ca. 150 to 450 m. (**B**) Area F2 in the central Amundsen Basin, 1 February 2020, 15:16 to 16:15 hours, 87.4°N, 95.8°E, showing a very weak DSL at ca. 100 to 200 m. (**C**) Area F3 in the inflow region of Atlantic water to the Arctic Basin, 19 May 2020, 03:16 to 04:15 hours, 83.3°N, 08.8°E, showing a DSL at ca. 250 to 500 m with smaller aggregations of fish. (**D**) Continental shelf waters above the Yermak Plateau, 28 June 2020, 13:42 to 14:41 hours, 81.9°N, 09.4°E, (station X), showing a larger fish aggregation at ca. 200 m and a dense DSL at ca. 350 to 500 m.

28 October 2019 and 19 May 2020, covering the DSL depth range as measured by the echosounder on the day of deployment (table S1). We are confident that these fish did not follow the bait down but actually were living in the DSL because the 38-kHz acoustic data showed that no fish-sized organisms occurred in the water column above the DSL (Fig. 2). Together, this extensive effort yielded 15 pelagic fish individuals from the DSL (Table 1). The fishing method did not affect catch success; eight fish were collected with longlines (table S1) and seven were collected with fishing rods. All fish were caught with the smallest hooks (Mustad 92247 Beak 4) and with squid as bait. Four of the fish were collected in October to November in area F1 (Figs. 1B and 2) in the central Amundsen Basin at 85.7°N to 86.0°N and 350 to 400 m of depth: three 43- to 68-cm-long Atlantic cod (Fig. 6, A to C) and one 33-cm-long ice cod (Fig. 6D). The other 11 fish were collected in May in area F3 (Figs. 1B and 2) in the inflow region of Atlantic water to the Arctic Basin near the Yermak

Plateau at 82.4°N to 83.3°N and 150 to 400 m of depth. These included three 32- to 57-cm-long Atlantic cod (Fig. 6, E to G), six 31- to 67-cm-long haddock (*Melanogrammus aeglefinus*), and two 40- to 54-cm-long beaked redfish (*S. mentella*).

In addition to the 15 pelagic fish, one 25-cm-long black seasnail (*Paraliparis bathybius*), a deep water demersal (bottom-feeding) fish of no commercial interest, was collected with a 1-m-diameter 150-µm-mesh zooplankton ring net towed between 2000 and 200 m of depth at 87.5°N, 95.1°E (area F2; Figs. 1B and 2). Despite the large sampling effort, no pelagic fish were caught in the region with low backscatter on the Fram Strait side of the Amundsen and Nansen Basins (Figs. 1B and 2). However, in the water column above the Yermak Plateau (station X just south of the CAO; Fig. 1B), another 42 fish were sampled in the DSL with longlines and fishing rods (33 haddock, 7 Atlantic cod, and 2 beaked redfish) during MOSAiC leg 4.
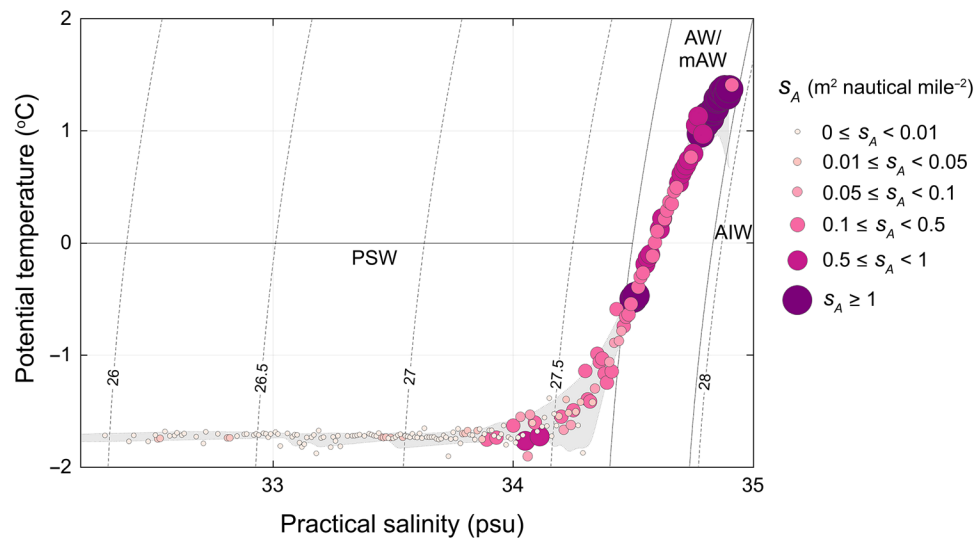
Fig. 4. The relationship between acoustic backscatter and water properties along the track of MOSAiC legs 1 to 3 (data S2). First, all s_A values in the entire dataset were averaged over 3.5-day intervals and 10-m-depth regular grid covering the water column between 0 and 600 m. A 3.5-day time interval was used because the potential temperature and salinity data were obtained from 60 CTD casts made in 207 days between 23 October 2019 and 17 May 2020 (on average, one CTD cast in 3.5 days). A 10-m-depth interval was used to include a reasonable number of s_A values within one grid. Then, the maximum s_A was selected from the 80 to 120 mean s_A values that were available for each 0.01 salinity interval between 32 and 35 practical salinity units (psu). One-meter binned temperature was interpolated between the surface and 600-m depth onto the same salinity intervals. The gray shading shows the temperature-salinity envelope, i.e., for each salinity the maximum and minimum temperature values. A low-pass filter was applied using a salinity cutoff of 0.03 psu. Curved dashed lines show potential density (in kilograms per cubic meter). Water mass temperature salinity envelopes differentiated by solid gray lines represent polar surface water (PSW), Atlantic water or modified Atlantic water (AW/mAW), and Arctic intermediate water (AIW).

The length of the three Atlantic cod from area F1 in the central Amundsen Basin (55 ± 12 cm; Fig. 6, A to C) did not differ significantly (*t* test, $P = 0.17$) from that of the three fish from area F3 in the inflow area of Atlantic water to the Arctic Basin (45 ± 12 cm; Fig. 6, E to G). Neither did the Fulton's condition index (K) of the fish differ significantly (*t* test, $P = 0.27$) between area F1 ($K = 0.72 ± 0.12$) and area F3 ($K = 0.82 ± 0.24$).

Population genetic analyses showed that of the six 3- to 6-year-old Atlantic cod from areas F1 and F3 (Fig. 6, A to C and E to G), five displayed the homozygotic *Pan* I^{BB} genotypes of the North-East Arctic cod (NEAC), which spawns along the northern coast of Norway. One specimen sampled in area F3 near the Yermak Plateau (MOSAiC fish ID number FR10054) displayed the heterozygotic *Pan* I^{AB} genotype, a hybrid between NEAC and Norwegian coastal cod (NCC) (Table 1).

Measurements of $\delta^{18}O$ in otolith increments of the six Atlantic cod revealed different life-history temperature reconstructions in fish from the two areas F1 and F3 (Fig. 7A). Two of the fish sampled in area F1 (MOSAiC fish ID numbers FR10002 and FR10003) had been exposed to cold waters typical of the Barents Sea surface water (1° to 2°C) during their early life stages. Fish FR10002 experienced warmer waters (4° to 6°C) resembling waters of the southern Barents Sea or west of Svalbard at ages 1 to 3 but showed a rapid movement into cold Arctic waters (0° to 1°C) in its past year. Fish FR10003 remained in cold water within the range of the northern Barents Sea and the Atlantic water layer of the CAO (1° to 2°C) and moved to even colder Arctic water (0° to 1°C) in the year of capture. The third fish from area F1 (MOSAiC fish ID number FR10027) had started out at higher water temperatures (>8°C), suggesting advection from the southern Norwegian Sea to the Fram Strait with warm surface currents, and ended up in the temperature range of

the Atlantic water layer of the CAO (1° to 2°C). In contrast, the three fish from area F3 in the inflow region of Atlantic water (MOSAiC fish ID numbers FR10054, FR10055, and FR10058) had followed warm surface currents through the Fram Strait into the colder Arctic Ocean during their life time, but there was no indication that they spent longer periods in Arctic waters below 2.5°C (Fig. 7A).

High numbers of prey items in the stomach and intestines of all six Atlantic cod from areas F1 and F3 (Table 2 and fig. S2) indicated that these fish had ingested substantial amounts of food before they were sampled. Fish parts (scales, otoliths, and fish bones) were identified in four of the six Atlantic cod, and one of them contained squid beaks. The guts of the three Atlantic cod from the central Amundsen Basin (area F1) contained between 22 and 172 *Themisto* spp., indicating a diet almost exclusively consisting of pelagic amphipods. Most of the *Themisto* spp. that could be identified to species level belonged to the Boreo-Atlantic species *Themisto abyssorum*. In the guts of Atlantic cod from the inflow region of Atlantic water to the Arctic Basin (area F3), *Themisto* spp. were also present, but they were not dominant (1 to 4 *Themisto* specimens per fish). Rather, all three fish from area F3 contained numerous chaetognath hooks, and fish FR10054 also contained pteropods, gelatinous hulls, and numerous green aggregates resembling appendicularian houses, suggesting a more varied diet than in the central Amundsen Basin (Table 2).

Animals observed in the DSL

Together, four confirmed fish detections were made from quantitatively analyzing 180 video recording hours from an ice-moored deep-sea camera ("FishCam") in the DSL, during six 5-day periods between 23 October and 7 November 2019 (at 375 ± 1 m of depth and
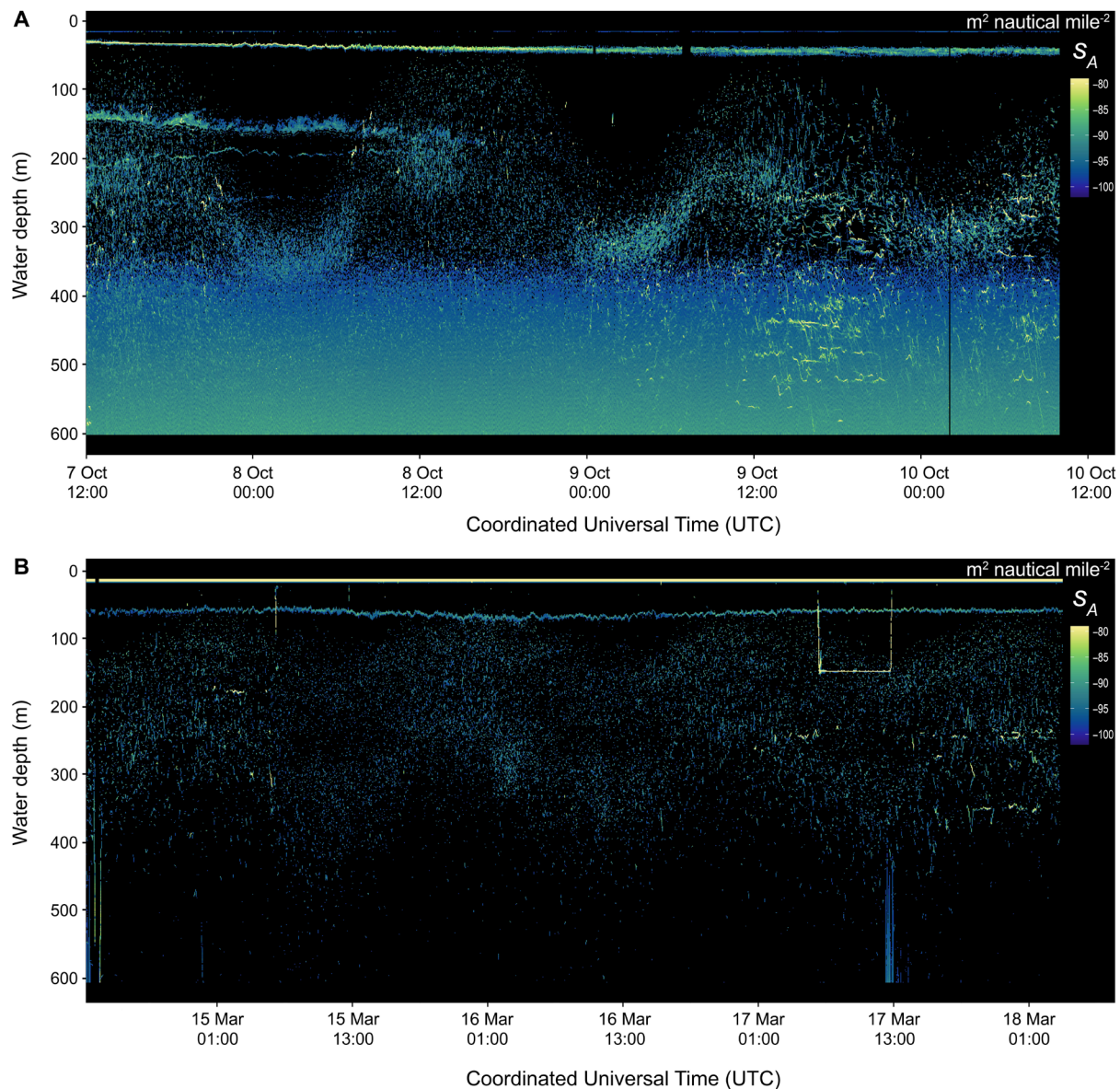
Fig. 5. Light-dependent DVM of the DSL in the CAO during the two seasonal twilight periods. (**A**) Three days with DVM during the transient phase with diel changes in light intensity when the polar day changed into the polar night in October 2019. The average geographical position was 85.0°N, 135.7°E, and the on-board time was Coordinated Universal Time (UTC) +7 hours. (**B**) Three days with DVM during the transient phase with diel changes in light intensity when the polar night changed into the polar day in March 2020. The average geographical position was 86.9°N, 13.4°E, and the on-board time was UTC +1 hour.

between 12 December 2019 and 11 March 2020 (at 213 ± 2 m of depth) (Figs. 1B and 2 and Table 3). During other times along the 3170-km-long track, the sea ice was too dynamic for deployment of the FishCam. One of the four fish (8 March 2020, 88.0°N, 25.5°E) was tentatively identified as the glacier lanternfish *Benthosema glaciale* (Figs. 2 and 6I and movie S1). The other three confirmed fish could not be identified to species level because they moved too fast. One of these fish was of the size of a lanternfish (ca. 5 cm), and the other two were larger (ca. 15 cm; Fig. 2). From their behavior in the periphery of the video recordings (movie S1), we conclude that they seemed to avoid the 6000-lumen (lm) white light-emitting diode (LED) lights of the FishCam. Numerous further potential

fish detections by the FishCam could not be confirmed due to the brevity of their appearance in the video recordings.

Armhook squid was common in the DSL. We identified >50 specimens on the video recordings, of which 36 by quantitatively analyzing 180 video recording hours (Figs. 1B and 6H and Table 3). The northernmost record was from 7 February 2020 at 87.6°N, 93.8°E, a depth of 214.6 m and a temperature of 1.1°C at a 4419-m-deep station in the central Amundsen Basin. Of these 36 squids, 33 were adults of different sizes, and three were juveniles. On the video recordings, the squids appeared very active and displayed various behaviors (movie S2). The frequency of the squid appearing in the video recordings decreased along the track, from six to seven individuals

Table 1. Fish sample data. Areas F1 and F2 are in the central Amundsen Basin, and area F3 is in the Fram Strait inflow region of Atlantic water to the Arctic Basin near the Yermak Plateau (Fig. 1B). –, not analyzed.

Species	Date	Area	Longitude (decimal °N)	Latitude (decimal °E)	Station depth (m)	MOSAiC fish ID number	Sampling device	Sex	Age (years)	Total length (cm)	Standard length (cm)	Weight (g)	Fulton's index (K)	G. morhua stock origin
A. glacialis	5 Nov 2019	F1	85.94	118.47	4410	FR10029	Longline	Male	4	33.2	30.6	210	0.57	–
G. morhua	29 Oct 2019	F1	85.67	125.21	4387	FR10002	Longline	Male	4	43.2	39.4	559	0.69	NEAC
G. morhua	29 Oct 2019	F1	85.67	125.21	4387	FR10003	Longline	Male	6	55.1	50.8	1036	0.62	NEAC
G. morhua	12 Nov 2019	F1	86.03	117.56	4412	FR10027	Fishing rod	Male	6	67.5	62.3	2600	0.85	NEAC
G. morhua	24 May 2020	F3	82.73	10.23	1862	FR10054	Fishing rod	Female	6	56.7	52.0	1306	0.72	NEAC/NCC
G. morhua	24 May 2020	F3	82.73	10.23	1862	FR10055	Fishing rod	Female	5	45.0	39.5	992	1.09	NEAC
G. morhua	27 May 2020	F3	82.38	8.30	1107	FR10058	Fishing rod	Immature	3	32.2	29.9	218	0.65	NEAC
M. aeglefinus	19 May 2020	F3	83.26	8.95	3713	FR10048	Longline	Female	–	57.7	52.9	1306	0.68	–
M. aeglefinus	19 May 2020	F3	83.26	8.95	3713	FR10050	Longline	Female	–	38.3	34.5	509	0.91	–
M. aeglefinus	19 May 2020	F3	83.26	8.95	3713	FR10051	Longline	Female	–	42.3	39.0	697	0.92	–
M. aeglefinus	19 May 2020	F3	83.26	8.95	3713	FR10052	Longline	Female	–	30.5	27.6	220	0.77	–
M. aeglefinus	24 May 2020	F3	82.73	10.23	1862	FR10053	Fishing rod	Female	–	67.1	61.2	2350	0.78	–
M. aeglefinus	24 May 2020	F3	82.73	10.23	1862	FR10057	Fishing rod	Female	–	38.6	35.4	527	0.92	–
S. mentella	19 May 2020	F3	83.26	8.95	3713	FR10049	Longline	Female	–	39.8	33.7	654	1.04	–
S. mentella	24 May 2020	F3	82.73	10.23	1862	FR10056	Fishing rod	Male	–	54.2	50.8	1082	0.68	–
P. bathybius	4 Feb 2020	F2	87.48	95.18	4424	FR10030	Ring net	–	–	24.5	23.0	130	0.88	–
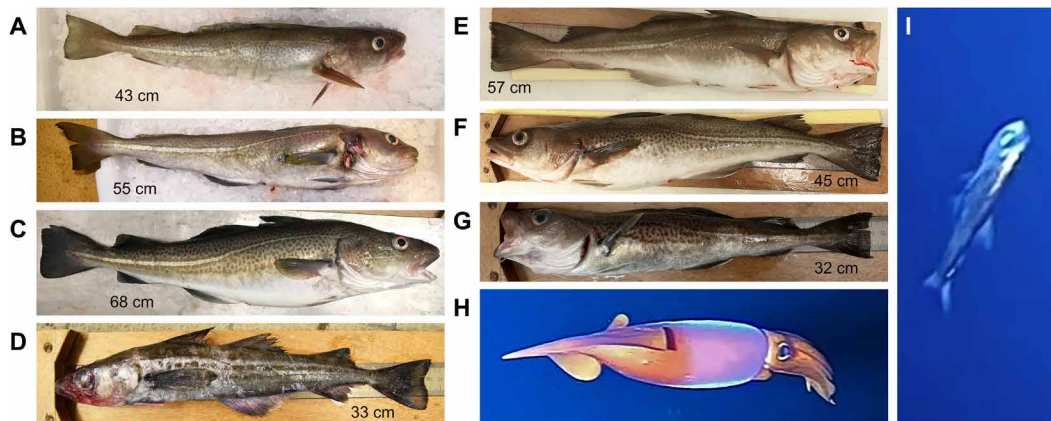
Fig. 6. Fish and squid sampled or recorded on video along the track of MOSAiC legs 1 to 3. (**A** to **C**) Atlantic cod from area F1. (A) FR10002. (B) FR10003. (C) FR10027. (**D**) Ice cod from area F1, FR10029. (**E** to **G**) Atlantic cod from area F3. (E) FR10054. (F) FR10055. (G) FR10058. (**H**) Armhook squid recorded on video, 16 December 2019, 86.6°N, 116.5°E; depth, 211.6 m; temperature, 1.14°C; estimated body length, ca. 20 to 30 cm (extracted from movie S2). (**I**) Lanternfish, cf. *Benthosema glaciale*, recorded on video 8 March 2020, 88.0°N, 25.5°E; depth, 214.2 m; temperature, 0.68°C; estimated body length, ca. 5 to 10 cm. (extracted from movie S1). The total length of the sampled fish (A to G) is indicated in the photographs. Numbers (FR10…) are MOSAiC fish ID numbers (cf. Table 1).
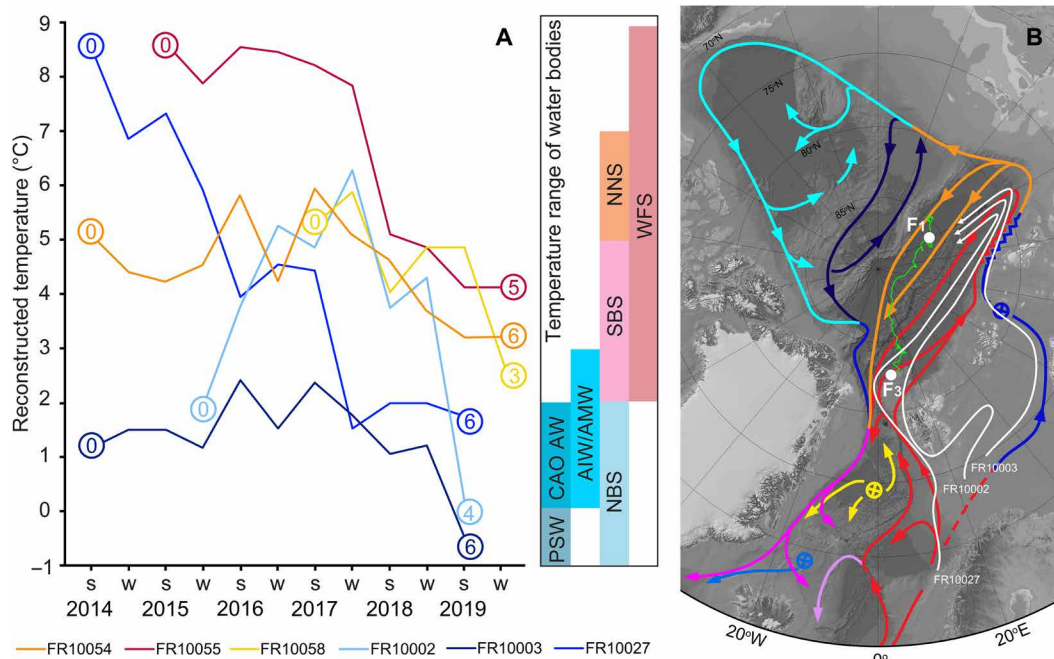
Fig. 7. Temperature reconstructions and potential migration pathways of Atlantic cod to the CAO (data S3). (**A**) Life-history temperature reconstructions for the six sampled Atlantic cod (*G. morhua*). The numbers in circles denote the birth year (0) and age at time of capture (3 to 6) for each individual fish. Three specimens were collected in area F1 in the central Amundsen Basin (MOSAiC fish ID numbers FR10002, FR10003, and FR10027, all with blue lines) and the other three in area F3 in the inflow region of Atlantic water to the Arctic Basin (MOSAiC fish ID numbers FR10054, FR10055, and FR10058, orange, red, and yellow lines). Ambient temperatures were reconstructed using δ^{18}O values measured in summer (s) and winter (w) increments of otoliths. The colored bars show temperature ranges of different water masses in the Arctic Ocean, and potential source areas for identifying possible migration routes of the six individuals during their life history: CAO AW, Atlantic water in the CAO; AIW/AMW, Arctic intermediate water or Atlantic modified water. Regional temperature ranges (50 to 200 m): NBS, northern Barents Sea; SBS, southern Barents Sea; NNS, northern Norwegian Sea; WFS, West Fram Strait. (**B**) Potential migration pathways of the three Atlantic cod sampled in area F1 to the CAO (white arrows) based on the temperature reconstructions in (A). The green line represents the 3170-km-long track (cf. Fig. 1). The colored arrows show the circulation in the subsurface Atlantic and intermediate layers of the Arctic Ocean (*26*).

per day in October to December to 2.4 per day in February, in concert with the weakening of the acoustic backscatter of the DSL (Fig. 2). In contrast to the fish, the armhook squid seemed to be attracted by the white camera lights. However, when getting very close to the light, they often released squid ink and tended to bump into the FishCam.

Prey items for both fish and squid predators were available in the Atlantic water layer. Amphipods, the main prey of the three Atlantic cod and the ice cod in the central Amundsen Basin (Table 2), were abundant in the DSL in October to November (Table 3). The FishCam recorded 35 to 120 amphipods per hour, while shrimps (decapods)

Table 2. Prey items identified in the guts of the seven sampled codfishes. The presence of food items in a fish gut (stomach and intestines combined) is indicated by "X" for areas F1 and F3 (Fig. 1B). For photographs of prey items, see fig. S2.

Area		Area F1 (central Amundsen Basin)				Area F3 (Atlantic inflow)		
Fish species		*G. morhua*	*G. morhua*	*G. morhua*	*A. glacialis*	*G. morhua*	*G. morhua*	*G. morhua*
MOSAiC fish ID number (cf. Table 1)		FR10002	FR10003	FR10027	FR10029	FR10054	FR10055	FR10058
Phylum (group)	**Taxon or item**							
Cnidaria (Hydrozoa)	Hydromedusae						X	
Crustacea (Copepoda)	*Metridia longa*				X			
Crustacea (Amphipoda)	*C. guilelmi*		X	X	X			
	Themisto spp.	X	X	X	X	X	X	X
	Eusirus holmii						X	
	Other Amphipoda					X	X	
Crustacea (Decapoda)	Shrimp parts			X	X	X	X	
Mollusca (Pteropoda)	*Clione limacina*					X		
	Limacina sp.					X		
Mollusca (Cephalopoda)	Squid beaks						X	
Chaetognatha (Sagittoidea)	Chaetognath parts					X	X	X
Chordata (Appendicularia)	Appendicularia parts					X		
Chordata (Actinopterygii)	Fish parts (scales, otoliths, and fish bones)	X			X	X	X	X
Number of different prey items		2	2	3	5	8	8	3

were less abundant with only 1.4 to 3.6 per hour. Further along the track, from December to March, amphipods were less abundant (7 to 15 per hour), while decapods remained at a similar level (1.0 to 2.7 per hour).

Overall, copepods, chaetognaths, and jellyfish dominated the zooplankton community in the central Arctic DSL as observed in the video recordings. Among the jellyfish, we identified three species of siphonophores: *Dimophyes arctica*, *Rudjakovia plicata*, and *Marrus orthocanna* (Table 3, fig. S3, and movie S3). We focused on siphonophores because the two physonect species, *R. plicata* and *M. orthocanna*, have gas inclusions in their pneumatophores and could potentially contribute to acoustic backscatter. The two smaller species, *D. arctica* and *R. plicata*, were common with maxima of 23 individuals of *D. arctica* passing the video camera per hour in December and 21 individuals of *R. plicata* per hour in March. *M. orthocanna* was not observed in four of the six time periods studied and was recorded at much lower frequencies: 0.4 and 0.3 per hour in January and March, respectively (Table 3). *R. plicata* and *M. orthocanna* are similar in shape, but *M. orthocanna* was usually about two to five times the size of the up to ca. 15-cm-long *R. plicata* (fig. S3). Six in situ measurements of the pneumatophores in physonect siphonophores showed that the pneumatophore volume varied between 0.05 and 0.62 mm^3 (means ± SD = 0.35 ± 0.24 mm^3, $n = 6$) (fig. S4). Assuming that the gas inclusion volume is one-third of the pneumatophore volume (*25*), the gas inclusion would have a mean equivalent spherical diameter (ESD) of 0.57 ± 0.16 mm (table S2).

DISCUSSION
The central Arctic DSL
Our acoustic data constitute the first coherent scientific hydroacoustic survey crossing the CAO. The weak but consistent DSL along the 3170-km-long track agrees with the central Arctic DSL that was found in summer 2016 at 13 discrete hydroacoustic stations over a transect from 84.4°N in the Nansen Basin, across the North Pole (90.0°N), to 82.4°N in the Canada Basin (*12*). The depth interval of our summer DSL (300 to 500 m) matched that of the central Arctic DSL observed in summer 2016. The signals consisted of acoustic tracks of individual targets indicative of small mesopelagic fish or smaller organisms grouped together. However, in area F1, we additionally observed (very few) tracks indicative of larger targets that possibly could be Atlantic cod or ice cod since we caught these species in this area. In the earlier study (*12*), it was hypothesized that the acoustic tracks of individual targets in the central Arctic DSL represented polar cod and/or ice cod with an average body length of 15.4 cm. This might be the case, but, unfortunately, the two 15-cm-long fish observed in our video recordings could not be identified to species level. Possibly, the smallest hooks we used for deep line fishing were still too large for catching these small fish, or they were not hungry or interested in the bait presented. In both studies, the central Arctic DSL was confined to the Atlantic water layer, and it was notably weaker on the Fram Strait side of the Amundsen and Nansen Basins. This reduction in acoustic backscatter coincided with decreasing zooplankton and armhook squid abundances in our video recordings and appeared to be closely related to

Table 3. Abundance of nekton and selected zooplankton analyzed in the video recordings (data S4). Data were analyzed for six periods, each containing five successive days with uninterrupted video data collection, divided over the time period that the FishCam delivered data. The dominant zooplankton groups in all video recordings were copepods, chaetognaths, and jellyfish (not counted). Only zooplankton groups relevant for the present study were included in the quantitative analyses of the video recordings. These consisted of siphonophores (fig. S3) because some species (*R. plicata* and *M. orthocanna*) may contribute to acoustic backscatter, and amphipods and decapods because these were the dominant zooplankton food items identified in the fish guts (Table 2).

Time period	24–28 Oct 2019	2–6 Nov 2019	13–17 Dec 2020	17–21 Jan 2020	5–9 Feb 2020	6–10 Mar 2020
Average geographical position						
Average latitude (decimal °N)	85.48	85.91	86.61	87.45	87.64	87.96
Average longitude (decimal °E)	127.43	119.87	117.30	97.87	93.84	26.02
Average water depth (m)	4370	4315	4403	4030	4319	3722
Environmental data (calculated from the daily means ± SD, n = 5 days)						
Deployment depth (m)	375.0 ± 1.1	375.2 ± 0.9	214.0 ± 1.4	213.8 ± 1.5	214.6 ± 0.1	213.3 ± 1.5
Drift speed ice floe (knots)	0.21 ± 0.09	0.22 ± 0.06	0.19 ± 0.10	0.19 ± 0.10	0.15 ± 0.04	0.28 ± 0.08
Water temperature (°C)	1.39 ± 0.02	1.33 ± 0.01	1.17 ± 0.02	1.13 ± 0.01	1.13 ± 0.01	0.61 ± 0.08
Salinity (psu)	30.3 ± 0.0	30.2 ± 0.0	30.0 ± 0.0	29.9 ± 0.0	29.9 ± 0.0	29.4 ± 0.1
Nautical area scattering coefficient (s_A)	4.65 ± 3.07	7.90 ± 1.98	0.07 ± 0.07	0.45 ± 0.26	0.33 ± 0.20	0.06 ± 0.09
Number of organisms per screen	50–100	25–100	50–100	25–50	10–50	<10
Abundance nekton (fish and squid), average number of observations per hour of video recording						
Number of hours analyzed	40	40	40	20	20	20
Fish	0.00	0.00	0.05	0.00	0.05	0.05
G. fabricii (armhook squid)	0.25	0.30	0.28	0.20	0.10	0.00
Abundance zooplankton, average number of observations per hour of video recording						
Number of hours analyzed	10	10	10	10	10	10
D. arctica (siphonophore)	8.4	6.7	23.4	17.4	11.5	3.0
R. plicata (siphonophore)	2.0	0.8	5.8	7.6	8.2	21.3
M. orthocanna (siphonophore)	0.0	0.0	0.0	0.4	0.0	0.3
Amphipods	120.4	35.3	6.9	15.4	13.2	12.3
Decapods	1.4	3.6	1.2	1.0	2.7	2.4
Ratio amphipods/siphonophores	11.6	4.7	0.2	0.6	0.7	0.5

the cooling and freshening of the Atlantic water layer after mixing with cold Arctic water when approaching the outflow area from the Arctic Basin to the Atlantic Ocean (*26*, *27*).

The DVM of the central Arctic DSL during the two short seasonal twilight periods agrees well with the general concept of synchronized shifts in depth distribution of pelagic scatterers in response to diel changes in light availability (*7*, *10*). Similar to our results, DVM of the zooplankton in the upper 90-m surface layer near Svalbard (79°N to 82°N) persists into the polar night as long as some sunlight was still reflected at the horizon (*28*). This signifies a high sensitivity of the pelagic community to very subtle changes in light availability. However, under the constant light conditions of the polar day and the polar night, we found that DVM ceased. The same phenomenon was previously observed for zooplankton in the upper 60-m surface layer during the polar night very close to the North Pole (89°N) (*29*). In summer, avoidance of visual predation by diving mammals may be a possible reason for the central Arctic DSL to remain at depths below 300 m. However, the depth of the DSL is still within the diving reach of ringed seals (*30*), beluga whales (*31*), and narwhals (*32*). Hence, the DSL could support the survival of mammals in the North Pole area, including the hypercarnivorous

polar bear. Lunar vertical migration of the central Arctic DSL, with surface zooplankton sinking down to ca. 50 m at full moon (*33*), was not observed in our acoustic dataset but cannot be excluded until more detailed analyses of the surface water layer acoustics are made.

Even if we provide evidence that the central Arctic DSL does contain fish, based on a combination of acoustics, visual observations, and fish samples, our data do not allow a detailed estimate of the density and biomass of particular fish species. The visual observations and samples are too few for such estimations, and acoustic signals resembling those of small mesopelagic fish may also be partly caused by the gas-filled pneumatophores of physonect siphonophores (*25*, *34*). Backscatter from siphonophores would, in our data, be primarily attributed to the small (up to ca. 15 cm) species *R. plicata* and, to a minor extent, to the (in our analyses) very rare larger species *M. orthocanna*. The latter is able to reach a colony length of up to 2 to 3 m (*35*), but the specimens we observed in the FishCam video recordings were much smaller (usually <30 cm). On the basis of the in situ measured mean pneumatophore gas inclusion size of 0.57-mm ESD, we argue that the contribution of backscatter from siphonophores to our acoustic dataset is probably only marginal. The acoustic tracks of individual targets indicative of small mesopelagic

fish had a TS between −45 and −50 dB at 38 kHz. According to a theoretical model, a pneumatophore gas inclusion of 0.57 ESD would at 38 kHz have a TS of ca. −70 at 200-m depth and −85 dB at 500-m depth (*12*), i.e., below our analytical threshold of −65 dB. The 38-kHz backscatter strength of abundant zooplankton other than siphonophores was always below −65 dB. This applies also to armhook squid. Because of lack of gas inclusions and only a soft chitinous pen embedded in its body tissue, the squid would give much weaker echoes at 38 kHz than a similar-sized swim-bladdered fish. The predicted TS of a 10-cm-long squid in the mesopelagic zone would be around −80 dB, that of a 16.5-cm-long medusa would be around −90 dB, and that of a 1-cm euphausiid or a 1.5-mm copepod below would be around −120 dB (*34*). Hence, the expected TS at 38 kHz from squid and zooplankton was most likely too weak to obscure the backscatter of small mesopelagic fish.

The Atlantic water layer: A suitable habitat for pelagic nekton in the CAO

The unexpected occurrence of Atlantic cod and lanternfish and the unexpectedly wide distribution of armhook squid in the deepest Arctic Ocean Basin (the Amundsen Basin) suggest that the CAO may host many more Atlantic species than assumed before. This is possible because the Atlantic water layer provides a continuous pelagic habitat with suitable environmental conditions (temperature, >0°C) and food for the animals living in the central Arctic DSL, as well as connectivity between the deep Arctic basins. The circulation of Arctic water in the CAO can be seen as an extension of the Atlantic habitat into the CAO in-between two colder (temperature, <0°C) upper and lower Arctic water layers. The Atlantic water layer is an integral part of ocean circulation in both the Eurasian and Amerasian Basins, but the two-branched inflow of warm and saline Atlantic water is roughly 12 km^3 s^{-1} (*26*), more than 10 times larger in volume than the Pacific inflow to the CAO. Hence, the Atlantic water circulation can be considered a "vein of life" stretching from the Fram Strait and northern Barents Sea through all deep basins of the CAO. We showed that large aggregations of Atlantic predatory fish species (Atlantic cod, haddock, and beaked redfish) were standing at the Yermack Plateau near the Fram Strait gateway in May to June and partly enter the CAO with the Atlantic inflow. It is then not unlikely that these fish end up in the CAO with the Atlantic water circulation north of the Barents, Kara, and Laptev Seas, respectively, as we showed for Atlantic cod. We report here the northernmost records of three large Atlantic predatory fish, one Arctic endemic planktivorous/piscivorous fish, and one small Atlantic planktivorous fish typical of mesopelagic DSLs.

Atlantic cod

We sampled three healthy Atlantic cod in the central Amundsen Basin. This establishes that the Atlantic cod can migrate into the Arctic Basin as far as 86°N and 126°E, considerably extending its previously known northernmost and easternmost distribution limits. The earlier reported northernmost distribution of Atlantic cod is from around 77.3°N in Northeast (NE) Greenland waters (*36*) and 82.0°N in the northern Barents Sea (*22*), while its easternmost distribution includes single specimens found in the southwestern Kara Sea (around 70°E) during warm years (*37*). Two of the three Atlantic cod we sampled had a typical length at age (*38, 39*). However, the one fish that had been exposed to Arctic temperatures for its entire 6-year life time (FR10003) was 11 cm shorter than the

other 6-year Atlantic cod (FR10027) that had spent only 2 years in Arctic temperatures, suggesting slower growth in colder temperatures. In all three Atlantic cod, the Fulton's condition index (*K*) was within the range known for Atlantic cod in the North Atlantic (*40*), exposing no indication of any prolonged resource limitation. This circumstance was confirmed by their well-filled guts, demonstrating that they survived by feeding on amphipods and small fish. An expansion of the Norwegian spawning stock of this Boreo-Atlantic species to the deep Arctic basins was so far not considered possible as the Atlantic cod was considered strictly shelf-associated (*22, 41*), i.e., it was assumed that a sojourn in the CAO would imply death. However, it was recently demonstrated that Atlantic cod can leave the shelf for an epipelagic life in the Fram Strait (*42*), and our results show that this species is able to survive outside the continental-shelf habitat even in the CAO.

In contrast to armhook squid (*24*), there is no evidence of a spawning population of Atlantic cod in the CAO. Rather, it must be assumed that the three specimens we sampled were immigrants because they were part of the NEAC stock. This population spawns along the coast of northern Norway, from where larvae and juveniles are advected to the Barents Sea or the Fram Strait west of Svalbard (*43*). On the basis of our life-history temperature reconstructions, we suggest two potential migration pathways of Atlantic cod from the known spawning areas of the NEAC stock into the CAO (Fig. 7B): (i) through the Barents Sea, as shown by persistent cold Arctic temperature exposure in fish FR10003, and (ii) through warmer waters west of Svalbard, as shown by the temperature profiles of fish FR10002 and FR10027. These two routes could support an Atlantic cod population in the CAO depending entirely on continuous immigration, as long as sufficient prey is available to sustain it.

Ice cod

The Arctic endemic ice cod we sampled at 85.9°N in the central Amundsen Basin could be expected this far north as this species has excellent adaptations to the cold Arctic environment (*44*). What is, however, notable with our observation is that it occurred far away from land at 350-m depth over a 4410-m-deep ocean basin because it has been assumed that ice cod is a shelf-associated species (*45*). On the Pacific side, sympagic ice cod has previously been caught at the edge of the CAO near the Mendeleyev Ridge by seismic blasts at ca. 15-m depth from the American drift station "Charlie" (77.1°N, December 1959) (*20*) and by baited hooks, nets, and a short gaff in the upper 25-m water column from the Soviet drift station "SP-16" (81.2°N, March 1969) (*18*). On the Atlantic side, ice cod has been reported from the area north of Svalbard up to 81.4°N (*45*) and up to 81.5°N in the North-East Water Polynya off NE Greenland (*46*). In the latter area, ice cod was the most abundant fish species, representing 44% of all fish caught, and was strictly planktivorous (*46*). The guts of our ice cod contained zooplankton but also some fish body parts, confirming earlier observations that ice cod is not strictly planktivorous and at a slightly higher trophic level than its relative the polar cod (*47*).

Lanternfish

Another northernmost record was established for a lanternfish (Myctophidae), tentatively identified from the video recording as glacier lanternfish. Myctophydae are small bioluminescent fish that typically occur in DSLs worldwide, where they contribute to a

large proportion of the biomass (*7*). They were thought to inhabit all oceans except the Arctic (*48*). However, two species, glacier lanternfish and rakery beaconlamp (*Lampanyctus macdonaldi*), have recently been reported from DSLs at the marginal ice zone north of Svalbard up to 81.6°N (*13*, *14*). Our record from the Atlantic water layer at 88.0°N suggests that lanternfish can potentially occur up to the North Pole.

Haddock and beaked redfish

While our records of Atlantic cod extend far into the Eurasian Basin, we sampled two other large predatory fish species, haddock and beaked redfish, in the inflow area of Atlantic water to the Arctic Basin up to 83.3°N. This is further north than their known distributions of up to 81.2°N at the southern Yermak Plateau and around 82.0°N in the northern Barents Sea (*22*, *42*, *49*). These two species were sampled, together with Atlantic cod, in combination with high acoustic backscatter in the inflow area and even higher backscatter at 81.9°N (station X) above the Yermak Plateau. High backscatter on the Yermak Plateau was also recorded in the first half of June 2017 (*15*). These data indicate that an overflow of northward migrating fish, standing at the gateway to the Arctic Ocean (at least in May to June), could constitute a source of Atlantic fish migrating into the CAO. With this in mind, it would not be unexpected if haddock and beaked redfish could sustain in the central Arctic DSL similar to Atlantic cod.

Armhook squid

Besides expected and unexpected fish, we found that the central Arctic DSL also hosts healthy armhook squid, and we conclude that squid probably constitutes a substantial part of the largely unknown nekton community of the CAO. On the Arctic shelves, armhook squid is the most abundant cephalopod (*35*, *50*, *51*). The habitat of our specimens was the central Arctic DSL over the >4000-m-deep Amundsen Basin at least up to 87.6°N, while the five previously recorded armhook squid in the CAO were found associated with submarine ridge areas. One 1.5-cm juvenile armhook squid was found in a plankton net tow at 500 to 300 m of depth on the Lomonosov Ridge (81.1°N; 1995) (Fig. 1B) (*23*). The other four previously recorded specimens were young and adult individuals from the Mendeleyev Ridge (79.6°N; 1962) and the Lomonosov Ridge (84.1° and 87.2°N; 1963 and 1968) (Fig. 1B) (*24*, *52*). It is unknown at which depth these four specimens were living because they were found (half) dead floating at the water surface in ice holes. One of the ice hole squids was a postspawning female, demonstrating that this species is able to reproduce in the CAO (*24*). This latter observation, together with our records of >50 armhook squids in different life stages, suggests that a spawning population of this species inhabits the CAO.

Ecological role of mesopelagic nekton in the CAO

The vertical carbon flux from the euphotic zone to deeper water driven by mesopelagic nekton (as part of the biological carbon pump) is very low in the CAO. This can be concluded from the combination of low acoustic backscatter and short twilight DVM time windows that characterizes the central Arctic DSL, in comparison with the much higher DSL backscatter and year-round DVM reported from other oceans (*7*, *53*). On the other hand, our results also disclose that the CAO does not differ much from all other oceans with respect to food web structure. We do not only confirm

the widespread distribution of the central Arctic DSL dominated by a mixture of zooplankton, cephalopods, and small mesopelagic fish, but we also found that an additional trophic level, large predatory nekton (Atlantic cod and armhook squid), is part of the pelagic food web of the CAO. However, the contribution of large predatory nekton to food web dynamics in the CAO remains to be quantified.

The marine ecosystems of the Arctic Ocean, including the CAO, are net beneficiaries of nutrients and biomass produced elsewhere by advection through the Pacific and Atlantic gateways (*54*). Advected Atlantic zooplankton contributes substantially to both the number of species and the zooplankton biomass found in the Eurasian Basin (*54*, *55*). Large migratory predators can be expected to follow this food source. Thus, despite low primary production of the CAO ecosystem, the central Arctic DSL in the Atlantic water layer may constitute a widespread niche with so far underestimated food supply, supporting low abundances of predatory fish and squid. Our stomach analyses revealed that macrozooplankton and small mesopelagic fish in the DSL constitute a key carbon source for these large pelagic predators. These findings close a prominent knowledge gap regarding the pelagic food web beneath the permanent pack ice of the CAO (*5*, *6*) and warrant a revision of the conceptual paradigms of carbon flux and ecosystem structure in the CAO.

At northern latitudes, matches between prey quantity and quality are crucial. The pelagic amphipods *Themisto* spp. and *Cyclocaris guilelmi* are predominantly carnivorous predators during both summer and winter in the *Calanus*-based Arctic food web (*56*) and provide lipid-rich food to the fish in the Atlantic water layer of the CAO. We show that amphipods are abundant in the DSL and that they are consumed by the fish living there. However, an open question is still how a visual predator, such as Atlantic cod, can survive the polar night in the CAO because foraging success is expected to be reduced in total darkness (*57*). Since the condition and gut content of the Atlantic cods from the central Amundsen Basin indicated that they were not starving in November, it seems not likely that darkness would limit the distribution of Atlantic cod in the CAO. Similarly, diet analyses of Atlantic and Arctic fish from the Svalbard area have shown that gadoids (Atlantic cod, haddock, and polar cod) are well capable of capturing pelagic prey during the polar night (*28*). This raises the question as to how species known to be visual predators during other times of the year are able to find their prey in darkness. One answer could be bioluminescence. However, the main prey found in our cod stomachs (*T. abyssorum*) is reportedly nonluminescent (*58*).

Climate change and possible future fisheries

At first sight, our records of Atlantic cod in the central Amundsen Basin provide no evidence of a recent expansion of this species into the CAO with climate change. The circulation of the comparatively warm and salty Atlantic water in the CAO (*26*, *27*) has existed for at least 14 million years (*59*), and the absence of Atlantic cod from the CAO in the past cannot be proven. However, we cannot exclude the possibility that connectivity between the CAO and Atlantic species (Atlantic cod, haddock, beaked redfish, and probably others) has only recently emerged as a result of "Atlantification" of the Arctic shelf seas, i.e., the northward expansion of Atlantic species distributions with climate change. Many fish species have recently shifted hundreds of kilometers northward in the Barents Sea and Fram Strait area (*22*, *49*). These northward expansions can be coupled to

the substantially greater role for Atlantic inflows to the Arctic Basin due to recent ice reductions, weakening of the halocline, and shoaling of the Atlantic water layer, which has allowed progressively deeper winter ventilation in the ocean interior in the eastern Eurasian Basin (*60, 61*).

Climate change may thus trigger or increase the immigration of Atlantic nekton into the CAO. However, even if more Atlantic prey would be advected through increased inflow (e.g., *T. abyssorum*) together with the nekton, the capacity of the CAO ecosystem to support larger fish stocks is without doubt rather limited. On the shelves, the northward expansion of Atlantic fish communities is fueled by increasing primary production (*62*). In the CAO, annual net primary production is, on average, only 13 g of C m^{-2} year^{-1} (*63*). There is no indication of a substantial increase in the biological productivity of the CAO between 1991 and 2015 (*64*), and a potential future increase in productivity is expected to remain low in the CAO due to stratification-induced nutrient limitation (*65*). Therefore, we expect that the CAO can support only a low biomass of Atlantic fish compared to adjacent Arctic shelf seas such as the Barents Sea. This fish biomass is not expected to become high enough to support any sustainable commercial fishery in the CAO. Thus, despite their potential ecological relevance, fish stocks in the CAO will likely remain economically irrelevant—at least during the coming decades while the summer ice cover continues to withdraw. The here reported new findings highlight that scientific knowledge about the CAO ecosystem still holds large gaps. Therefore, we strongly recommend maintaining the present science first policy under international protection (*9*), before considering any harvesting of living resources in the high seas portion of the CAO.

MATERIALS AND METHODS
Hydroacoustics
We continuously collected water column acoustic backscatter data along the track between 1 October 2019 and 27 May 2020 using a Simrad EK60/80 echosounder and five transducers mounted at 11-m depth on the hull of the ship. This paper reports the results from the 38-kHz Simrad ES38B, the main frequency used for fish studies. This transducer was operated in continuous wave mode and pulse length 1.024 ms, 15 pulses min^{-1}. The data were logged directly onto large storage arrays in the Simrad raw format. Throughout the 8-month drift track, we inspected the accuracy of the data collection several times per day. On 27 April 2020, we calibrated the equipment according to standard procedures (*66*) through the ship's moon pool using a standard tungsten carbide sphere (38.1 mm) with the aid of an underwater remotely operated vehicle (ROV). Sound velocity was determined from a CTD cast (SBE-911 plus). We regularly inspected the surface of the transducer using an ROV with high-definition (HD) cameras. Sporadic noise due to interferences from instruments running temporarily on the MOSAiC ice floe (e.g., portable Wide-Band Autonomous Transceivers) and backscatter traces of other equipment temporarily operated from the ship (e.g., bottom profiler) were removed using the Echoview 10 postprocessing software. For further processing, the 38-kHz samples were averaged over 60 s × 0.25 m using Echoview's "resample" algorithm. For characterization of the acoustic backscatter from swim-bladdered fish, a lower threshold of −65 dB was applied to the data before echo integration. Backscatter from the interface layer between water masses was also removed from the analysis.

Video recordings
We used a deep-sea video system (FishCam, MacArtney Germany GmbH, Kiel, Germany) to optically monitor the DSL. The FishCam was deployed to detect nekton and physonect siphonophores generating acoustic signals that can be confused with those of swim-bladdered fish. The FishCam consisted of a frame with a mini CTD monitoring salinity, temperature, and depth every 10 s; two Luxus High-Power LED lamps of 6000 lm each; and two HD Internet Protocol cameras, one looking sideward and one looking downward into the water column. The system was moored from the ice about 500 m from the ship and connected to a personal computer on the ship running the PortVis (Serial Port and Video Stream Visualizer) software, version 2.1. The deployment depth slightly varied depending on water currents and the drift speed of the MOSAiC ice floe. The mean depth (±SD) was 375 ± 1 m (range, 369 to 376 m; n = 130,631 mini-CTD depth measurements) in the lower part of the Atlantic water layer between 23 October and 7 November 2019 and—after the DSL had shifted upward within the Atlantic water layer in the polar night—at 213 ± 2 m (range, 194 to 215 m; n = 692,723) between 12 December 2019 and 11 March 2020. During deployment of the FishCam, there were times that electricity and data cables temporarily broke off because of excessive ice dynamics or animal disturbance, and from 7 November to 12 December 2019 and 11 March to 27 May 2020, the sea ice was too dynamic for deployment of the FishCam, and no data exist for these time periods.

Video data analysis
Divided over the operation time of the FishCam, six periods of five successive days without disturbances were selected for detailed analysis of the video recordings. Together, 180 video recording hours were studied in real-time mode because the nekton moved very fast and could be missed even at double speed. Nekton was observed within ca. 0 to 3 m from the camera objective, and zooplankton was observed within ca. 0.0 to 0.6 m. The drift speed of the MOSAiC ice floe was variable, and most of the smaller zooplankton (e.g., copepods and small jellyfish) was unrecognizable at higher drift speed. The quantitative analyses (number of individuals passing the camera per hour) were made for those organisms that were relevant for the present study: nekton, siphonophores (some of which give acoustic backscatter), and amphipods and decapods (as food items for the nekton). Each of these organism groups has group-typical continual movements that could easily be recognized on the video recordings. During operation of the FishCam, the camera lights were turned on 10 s after the cameras were turned on to observe whether any animals would flee the light, but during the detailed analyses of the video recordings, no organisms were observed to flee as a result of turning on the lights. We also tested whether different light:dark periods (5:55, 15:15, and 55:5 min) would influence the occurrence of the organisms in the recordings. This was not the case: All species mentioned in the present study (Table 3) turned up in the video recordings independent of the length of the light:dark periods.

Fish sampling
We deployed 35 longlines and >300 fishing rods to sample fish (table S1). The longlines generally covered the whole DSL between 200 and 475 m of depth with baited hooks. The longlines were lowered into the water from a hole in the sea ice with a 200-m

Dyneema line carrying a weight at its lower end. The longline itself consisted of a 275-m-long fishing line with weights. Together, the weights attached to the longline added up to ca. 1.5 kg. To target a wide range of potential fish species and sizes, we applied three different standard salt water hook sizes: "large" = Owner Mutu Light 5114-5/0, "medium" = Owner Mutu Light 5114-3/0, and "small" = Mustad 92247 Beak 4. Shrimp (*Pandalus borealis*) and squid (*Ilex* sp.) were used as bait. The three hook sizes and two bait types were used 1.8 m apart in the sequence "large hook/shrimp, medium hook/shrimp, small hook/shrimp, large hook/squid, medium hook/squid, small hook/squid", thus covering 10.8 m of the longline length. This sequence was repeated throughout the depth of the DSL as seen on the echosounder. The longlines were deployed for ca. 24 hours before retrieval. The fishing rods were equipped with 600- to 700-m longlines and the same hook sizes and baits as the longlines.

Fish sample elaboration

The fish were photographed with a digital camera immediately after retrieval on board. We measured the total length (the length of the fish from the tip of the mouth to the end of the tail fin) and standard length (the length of the fish from the tip of the mouth to the end of the spine) to the nearest millimeter below. The fresh weight of the fish was measured with a scale (Kern) with a precision of 0.01 g. Subsequently, we sampled fin clips, otoliths, and fish organs for later analyses. The fin clips, stomachs, and intestines were preserved in molecular-grade ethanol, and the otoliths were air-dried and stored in Eppendorf tubes at 4°C. After extraction of all inner organs, we measured the eviscerated weight. Fulton's condition index (K) was calculated as $K = 100 \times FW/(TL)^3$, where FW represents the fresh weight with all organs (in grams) and TL is the total length (in centimeters).

Fish age determination

Otolith sections were made by breaking the otoliths through the core and embedding both pieces in VISCOVOSS GTS polyester resin. Sections of 0.5 mm were cut with a double-bladed diamond saw at the end of each otolith break line. Two otolith sections were recovered from each otolith, where feasible, and glued to a glass slide. High-resolution photographs of the otoliths were taken under a stereo microscope (Leica M205) connected to a digital imaging system based on the software Leica Application Suite, version 4.12. On the basis of the sequence of translucent and opaque "rings," we determined the age of the fish by blind reading performed by two independent age readers.

Fish gut content analysis

Before microscopic analysis, the ethanol-preserved fish stomach and intestines were opened with a scalpel, and the content was rinsed through a 30-μm gauze. The gut content was identified to the lowest possible taxon and enumerated using a stereo microscope (Leica M205) connected to a digital imaging system based on the software Leica Application Suite, version 4.12. We produced high-resolution photographs of animals, amphipod telsons, and any conspicuous items in the samples. A minimum number of prey items in each fish gut (stomach and intestines combined) was estimated for several prey taxa. Numbers of amphipods were recorded by adding the numbers of complete animals and the numbers of identifiable amphipod pleons. Minimum fish numbers were estimated in terms of whole bodies plus the number of free otoliths divided by two.

When only fish scales were present, a minimum number of one fish was assumed. Minimum numbers of chaetognaths were estimated on the basis of the number of complete heads.

Atlantic cod stock identification

High-quality DNA of fin clips of the six Atlantic cod (MOSAiC fish ID numbers FR10002, FR10003, FR10027, FR10054, FR10055, and FR10058) and one ice cod specimen as outgroup (FR10029) was extracted using QIAGEN's DNeasy Blood & Tissue kit (QIAGEN, Germany) after initial proteinase K digestion and grinding with a Teflon pestle. Polymerase chain reaction (PCR) was conducted following a fixed protocol (*67*). We used a universal forward primer (PanI-2-PIG-F): 5′- GTTTCTTTGACAGCGCTTGGCAAATGAA; and specific reverse primers: a *Pan* I^A–specific 5′FAM-labeled reverse primer (PanIA-FAM-R), 5′-GCT TAAGCAGATATCG-CAGTAGTTTC; and a *Pan* I^B–specific 5′HEX-labeled reverse primer (PanIB-HEX-R), 5′-TTAAGCAGATCTCGCAGTAGTTTT. PCR conditions comprised: 200-μm deoxynucleotide triphosphates, 300 nm of each primer, 0.2 U of 5′Taq polymerase (Eppendorf, Germany), 10 × 5′ PCR buffer (Eppendorf, Germany), and 30 to 70 ng of genomic DNA. PCR was run using initial denaturation at 94°C for 5 min, 94°C for 10 s, 60°C for 10 s, and 72°C for 30 s. The program was run for 30 cycles. PCR products were diluted 1:100 in HiDi formamide (Applied Biosystems, ABI) including a 1:100 dilution of the GeneScan 500 ROX Size Standard (ABI) and run on an ABI PRISM 3130 XL Genetic Analyzer (ABI). Sequence analysis was performed using ABI's Genemapper software (v4.0, ABI). The six specimens of Atlantic cod were allocated to the respective Atlantic cod stocks (North East Arctic cod, NEAC, NCC, and their hybrids) by allele specific PCR analysis of the pantophysin I (*Pan* I) locus (*68*). The *Pan* I^B allele is predominant in the NEAC stock, while *Pan* I^A dominates in the NCC stock.

Atlantic cod life-history temperature reconstructions

From the otolith sections used for fish age determination, opaque and translucent areas corresponding to summer and winter increments, respectively, were micromilled with a 0.8-mm diamond encrusted drill bit to a depth of 100 μm. Otolith powder from each increment was analyzed for δ^{18}O and δ^{13}C values on a Thermo Fisher 253 Plus gas isotope mass spectrometer connected to a Kiel IV automated carbonate preparation device at the MARUM, Center for Marine Environmental Sciences, University Bremen (Germany). Data were reported according to the usual delta notation versus a Vienna Pee Dee Belemnite (V-PDB) standard. The instrument was calibrated against the NBS 19 calcite standard. Over the measurement period, the SDs of the house standard were 0.02 per mil (‰) for δ^{13}C and 0.07‰ for δ^{18}O. Otolith δ^{18}O values were used to reconstruct ambient temperatures (T in °C) with an equation established for Atlantic cod (*69*) in controlled experimental settings: $T = (\delta C - \delta W) \times 0.2^{-1} + 19.5$, where δC is the otolith δ^{18}O value and δW is the mean Atlantic water δ^{18}O value of 0.2345‰ according to the Global Seawater Oxygen-18 Database, version 1.22 (https://data.giss.nasa.gov/o18data). Potential migration pathways of Atlantic cod to the CAO were based on temperature reconstructions and known temperatures of different water masses.

Measurement of the pneumatophore size of siphonophores

For measuring the pneumatophore size of physonect siphonophores, we used high-resolution images that were taken in situ with the

optical plankton recorder "Lightframe On-sight Keyspecies Investigation" (LOKI), iSiTEC, Bremerhaven, Germany. The LOKI consists of a plankton net (150-μm mesh size, 0.28-m^2 net opening covered by a 1-cm mesh net), which leads organisms and particles into a narrow flow-through chamber. Here, they are illuminated by a Power-LED flash (70000 lm) and photographed by a 6.1 MPix black-and-white charge-coupled device camera (Prosilica GT 2750, Allied Vision Technologies GmbH, Stadtroda, Germany) at a maximum rate of 19.8 frames per second (fps). A connected computer unit immediately scans the photographs for objects (software "LOKIRecorder," Medea AV, Germany) and saves images of encountered objects. The LOKI was deployed 15 times between 10 November 2019 and 20 February 2020 through an ice hole on the starboard side of the ship at a speed of 0.5 m s^{-1} to a maximum depth of 1000 m. The frame rate of the camera varied between 2 and 19.8 fps. Five of the images showed physonect siphonophores with a visible and measurable pneumatophore. A sixth pneumatophore image occurring in an LOKI cast from Fram Strait taken after 27 May 2020 was used as well. The size of the pneumatophores was measured using the GNU Image Manipulation Program GIMP (www.gimp.org) and converted into square millimeters using the camera's conversion factor of 1029.8 pixels cm^{-1}. The pneumatophores were observed from the side and apparently had a trapezoid to elliptical shape and a length:width ratio of ca. 1:2. The pneumatophore volume (V) was calculated assuming an overall ellipsoid shape according to the formula: $V = 4/3\pi \times (W/2)^2 \times L/2$, where W is the width (diameter) and L is the length.

CTD data processing and quality check

A CTD probe was operated twice per week from the surface to 4000-m depth. The CTD was equipped with the standard SBE911plus setup including double sensors for temperature and conductivity. The CTD data were checked for spikes manually, using the standard, SBEDataProcessing-based, routines at the Alfred Wegener Institute, Germany. The accuracy of the temperature data is better than ±0.01°C. The accuracy of the salinity data is better than ±0.01. Throughout this study, we used practical salinity and potential temperature referred to the ocean surface; both were derived using the TEOS-10 GSW (www.teos-10.org/software.htm) toolbox software.

SUPPLEMENTARY MATERIALS

Supplementary material for this article is available at https://science.org/doi/10.1126/sciadv.abj7536

REFERENCES AND NOTES

1. E. Post, R. B. Alley, T. R. Christensen, M. Macias-Fauria, B. C. Forbes, M. N. Gooseff, A. Iler, J. T. Kerby, K. L. Laidre, M. E. Mann, J. Olofsson, J. C. Stroeve, F. Ulmer, R. A. Virginia, M. Wang, The polar regions in a 2°C warmer world. *Sci. Adv.* **5**, eaaw9883 (2019).
2. R. Kwok, Arctic sea ice thickness, volume, and multiyear ice coverage: Losses and coupled variability (1958–2018). *Environ. Res. Lett.* **13**, 105005 (2018).
3. PAME, *Large Marine Ecosystems (LMEs) of the Arctic Area: Revision of the Arctic LME Map* (PAME International Secretariat, ed. 2, 2013).
4. J. S. Christiansen, C. W. Mecklenburg, O. V. Karamushko, Arctic marine fishes and their fisheries in light of global change. *Glob. Chang. Biol.* **20**, 352–359 (2014).
5. T. I. Van Pelt, H. P. Huntington, O. V. Romanenko, F. J. Mueter, The missing middle: Central Arctic Ocean gaps in fishery research and science coordination. *Mar. Policy* **85**, 79–86 (2017).
6. P. Snoeijs-Leijonmalm, H. Flores, F. Volckaert, B. Niehoff, F. L. Schaafsma, J. Hjelm, J. Hentati-Sundberg, A. S. Niiranen, A. S. Crépin, H. Österblom, *Review of the Research Knowledge and Gaps on Fish Populations, Fisheries and Linked Ecosystems in the Central Arctic Ocean (CAO)* (EU Publications, European Commission, 2020); https://op.europa.eu/en/publication-detail/-/publication/aae1e59e-46fe-11ea-b81b-01aa75ed71a1/language-en.
7. X. Irigoien, T. A. Klevjer, A. Røstad, U. Martinez, G. Boyra, J. L. Acuña, A. Bode, F. Echevarria, J. I. Gonzalez-Gordillo, S. Hernandez-Leon, S. Agusti, D. L. Aksnes, C. M. Duarte, S. Kaartvedt, Large mesopelagic fishes biomass and trophic efficiency in the open ocean. *Nat. Commun.* **5**, 3217 (2014).
8. S. F. McWhinnie, The tragedy of the commons in international fisheries: An empirical examination. *J. Environ. Econ. Manage.* **57**, 321–333 (2009).
9. H. Hoag, Nations put science before fishing in the Arctic. *Science* **358**, 1235 (2017).
10. T. A. Klevjer, X. Irigoien, A. Røstad, E. Fraile-Nuez, V. M. Benítez-Barrios, S. Kaartvedt, Large scale patterns in vertical distribution and behaviour of mesopelagic scattering layers. *Sci. Rep.* **6**, 19873 (2016).
11. S. Kaartvedt, J. Titelman, Planktivorous fish in a future Arctic Ocean of changing ice and unchanged photoperiod. *ICES J. Mar. Sci.* **75**, 2312–2318 (2018).
12. P. Snoeijs-Leijonmalm, H. Gjøsæter, R. B. Ingvaldsen, T. Knutsen, R. Korneliussen, E. Ona, H. R. Skjoldal, C. Stranne, L. Mayer, M. Jakobsson, K. Gårdfeldt, A deep scattering layer under the North Pole pack ice. *Prog. Oceanogr.* **194**, 102560 (2021).
13. H. Gjøsæter, P. H. Wiebe, T. Knutsen, R. B. Ingvaldsen, Evidence of diel vertical migration of mesopelagic sound-scattering organisms in the Arctic. *Front. Mar. Sci.* **4**, 332 (2017).
14. M. Geoffroy, M. Daase, M. Cusa, G. Darnis, M. Graeve, N. S. Hernández, J. Berge, P. E. Renaud, F. Cottier, S. Falk-Petersen, Mesopelagic sound scattering layers of the High Arctic: Seasonal variations in biomass, species assemblage, and trophic relationships. *Front. Mar. Sci.* **6**, 364 (2019).
15. P. Priou, A. Nikolopoulos, H. Flores, R. Gradinger, E. Kunisch, C. Katlein, G. Castellani, T. Linders, J. Berge, J. A. Fisher, M. Geoffroy, Dense mesopelagic sound scattering layer and vertical segregation of pelagic organisms at the Arctic-Atlantic gateway during the midnight sun. *Prog. Oceanogr.* **196**, 102611 (2021).
16. H. Gjøsæter, R. Ingvaldsen, J. S. Christiansen, Acoustic scattering layers reveal a faunal connection across the Fram Strait. *Prog. Oceanogr.* **185**, 102348 (2020).
17. FiSCAO, *Final Report of the Fourth Meeting of Scientific Experts on Fish Stocks in the Central Arctic Ocean* (FiSCAO, 2017).
18. A. P. Andriashev, B. F. Mukhomediyarov, E. A. Pavshtiks, On mass congregations of the cryopelagic cod fishes (*Boreogadus saida* and *Arctogadus glacialis*) in circumpolar Arctic basins, in *Biology of the Central Arctic Basin*, M. E. Vinogradov, I. A. Melnikov, Eds. (Shirshov Institute of Oceanology, Academy of Sciences of the USSR, Nauka Science Press, 1980), pp. 196–211.
19. C. David, B. Lange, T. Krumpen, F. Schaafsma, J. A. van Franeker, H. Flores, Under-ice distribution of polar cod *Boreogadus saida* in the central Arctic Ocean and their association with sea-ice habitat properties. *Polar Biol.* **39**, 981–994 (2016).
20. V. Walters, Winter abundance of *Arctogadus glacialis* in the Polar Basin. *Copeia* **1961**, 236–237 (1961).
21. A. B. Hollowed, B. Planque, H. Loeng, Potential movement of fish and shellfish stocks from the sub-Arctic to the Arctic Ocean. *Fish. Oceanogr.* **22**, 255–370 (2013).
22. T. Haug, B. Bogstad, M. Chierici, H. Gjøsæter, E. H. Hallfredsson, Å. S. Høines, A. H. Hoel, R. B. Ingvaldsen, L. L. Jørgensen, T. Knutsen, H. Loeng, L. J. Naustvoll, I. Røttingen, K. Sunnanå, Future harvest of living resources in the Arctic Ocean north of the Nordic and Barents Seas: A review of possibilities and constraints. *Fish. Res.* **188**, 38–57 (2017).
23. K. N. Nesis, West-Arctic and East-Arctic distributional ranges of cephalopods. *Sarsia* **86**, 1–11 (2001).
24. R. E. Young, Evidence for spawning by *Gonatus* sp. (Cephalopoda: Teuthoidea) in the High Arctic Ocean. *Nautilus* **87**, 53–58 (1973).
25. E. G. Barham, Siphonophores and the deep scattering layer. *Science* **140**, 826–828 (1963).
26. B. Rudels, Arctic Ocean circulation, in *Encyclopedia of Ocean Sciences*, J. H. Steele, Ed. (Academic Press, 2019), pp. 211–225.
27. M.-L. Timmermans, J. Marshall, Understanding Arctic Ocean circulation: A review of ocean dynamics in a changing climate. *JGR Oceans* **125**, e2018JC014378 (2020).
28. J. Berge, P. E. Renaud, G. Darnis, F. Cottier, K. Last, T. M. Gabrielsen, G. Johnsen, L. Seuthe, J. M. Weslawski, E. Leu, M. Moline, J. Nahrgang, J. E. Søreide, Ø. Varpe, O. J. Lønne, M. Daase, S. Falk-Petersen, In the dark: A review of ecosystem processes during the Arctic polar night. *Prog. Oceanogr.* **139**, 258–271 (2015).
29. L. Hobbs, F. R. Cottier, K. S. Last, J. Berge, Pan-Arctic diel vertical migration during the polar night. *Mar. Ecol. Progr. Ser.* **605**, 61–72 (2018).
30. A. L. Von Duyke, D. C. Douglas, J. K. Herreman, J. A. Crawford, Ringed seal (*Pusa hispida*) seasonal movements, diving, and haul-out behavior in the Beaufort, Chukchi, and Bering Seas (2011–2017). *Ecol. Evol.* **10**, 5595–5616 (2020).
31. D. D. W. Hauser, K. L. Laidre, S. L. Parker-Stetter, J. K. Horne, R. S. Suydam, P. R. Richard, Regional diving behavior of Pacific Arctic beluga whales *Delphinapterus leucas* and possible associations with prey. *Mar. Ecol. Prog. Ser.* **541**, 245–264 (2015).
32. O. M. Tervo, S. Ditlevsen, M. C. Ngô, N. H. Nielsen, S. B. Blackwell, T. M. Williams, M. P. Heide-Jørgensen, Hunting by the stroke: How foraging drives diving behavior and locomotion of East-Greenland narwhals (*Monodon monoceros*). *Front. Mar. Sci.* **7**, 596469 (2021).

33. K. S. Last, L. Hobbs, J. Berge, A. S. Brierly, F. Cottier, Moonlight drives ocean-scale mass vertical migration of zooplankton during the Arctic winter. *Curr. Biol.* **26**, 244–251 (2016).

34. R. Proud, N. O. Handegard, R. J. Kloser, M. J. Cox, A. S. Brierly, From siphonophores to deep scattering layers: Uncertainty ranges for the estimation of global mesopelagic fish biomass. *ICES J. Mar. Sci.* **76**, 718–733 (2018).

35. K. A. Raskoff, R. R. Hopcroft, K. N. Kosobokova, J. E. Purcell, M. Youngbluth, Jellies under ice: ROV observations from the Arctic 2005 hidden ocean expedition. *Deep Sea Res. II* **57**, 111–126 (2010).

36. J. S. Christiansen, E. Bonsdorff, I. Byrkjedal, S. E. Fevolden, O. V. Karamushko, A. Lynghammar, C. W. Mecklenburg, P. D. R. Møller, J. Nielsen, M. C. Nordström, K. Præbel, R. M. Wienerroither, Novel biodiversity baselines outpace models of fish distribution in Arctic waters. *Sci. Nat.* **103**, 8 (2016).

37. A. V. Dolgov, Annotated list of fish-like vertebrates and fish of the Kara Sea. *J. Ichthyol.* **53**, 914–922 (2013).

38. G. Marteinsdottir, G. A. Begg, Essential relationships incorporating the influence of age, size and condition on variables required for estimation of reproductive potential in Atlantic cod *Gadus morhua*. *Mar. Ecol. Prog. Ser.* **235**, 235–256 (2002).

39. F. Vinje, M. Heino, U. Dieckmann, O. R. Godø, J. Mork, Spatial structure in length at age of cod in the Barents Sea. *J. Fish Biol.* **62**, 549–564 (2003).

40. L. G. S. Mello, G. A. Rose, Seasonal cycles in weight and condition in Atlantic cod (*Gadus morhua* L.) in relation to fisheries. *ICES J. Mar. Sci.* **62**, 1006–1015 (2005).

41. A. B. Hollowed, S. Sundby, Change is coming to the northern oceans. *Science* **344**, 1084–1085 (2014).

42. R. B. Ingvaldsen, H. Gjøsæter, E. Ona, K. Michalsen, Atlantic cod (*Gadus morhua*) feeding over deep water in the high Arctic. *Polar Biol.* **40**, 2105–2111 (2017).

43. G. Ottersen, B. Bogstad, N. A. Yaragina, L. C. Stige, F. B. Vikebø, P. Dalpadado, A review of early life history dynamics of Barents Sea cod (*Gadus morhua*). *ICES J. Mar. Sci.* **71**, 2064–2087 (2014).

44. A. L. Devries, C. H. C. Cheng, Antifreeze proteins and organismal freezing avoidance in polar fishes, in *Fish Physiology: The Physiology of Polar Fishes*, J. Steffensen, Ed. (Elsevier Inc., 2005), vol. 22, pp. 155–201.

45. M. Aschan, O. V. Karamuschko, I. Byrkjedal, R. Eienerroither, I. V. Borklin, J. S. Christiansen, Records of the gadoid fish *Arctogadus glacialis* (Peters, 1874) in the European Arctic. *Polar Biol.* **32**, 963–970 (2009).

46. L. Süfke, D. Piepenburg, C. F. von Dorrien, Body size, sex ratio and diet composition of *Arctogadus glacialis* (Peters, 1874) (Pisces: Gadidae) in the Northeast Water Polynya (Greenland). *Polar Biol.* **20**, 357–363 (1998).

47. J. S. Christiansen, H. Hop, E. M. Nilssen, J. Joensen, Trophic ecology of sympatric Arctic gadoids, *Arctogadus glacialis* (Peters, 1872) and *Boreogadus saida* (Lepechin, 1774), in NE Greenland. *Polar Biol.* **35**, 1247–1257 (2012).

48. V. Catul, M. Gauns, P. K. Karuppasamy, A review on mesopelagic fishes belonging to family Myctophidae. *Rev. Fish Biol. Fish.* **21**, 339–354 (2011).

49. M. Fossheim, R. Primicerio, E. Johannesen, R. B. Ingvaldsen, M. M. Aschan, A. V. Dolgov, Recent warming leads to a rapid borealization of fish communities in the Arctic. *Nat. Clim. Chang.* **5**, 673–677 (2015).

50. J. C. Xavier, Y. Cherel, R. Allcock, R. Rosa, R. M. Sabirov, M. E. Blicher, A. V. Golikov, A review on the biodiversity, distribution and trophic role of cephalopods in the Arctic and Antarctic marine ecosystems under a changing ocean. *Mar. Biol.* **165**, 93 (2018).

51. A. V. Golikov, M. E. Blicher, L. L. Jørgensen, W. Walkusz, D. V. Zakharov, O. L. Zimina, R. M. Sabirov, Reproductive biology and ecology of the boreoatlantic armhook squid *Gonatus fabricii* (Cephalopoda: Gonatidae). *J. Mollus. Stud.* **85**, 341–353 (2019).

52. K. N. Nesis, Squid *Gonatus fabricii* (Licht.) in the center of the Arctic Ocean. *Hydrobiol. J.* **7**, 76–79 (1971).

53. G. K. Saba, A. B. Burd, J. P. Dunne, S. Hernández-León, A. H. Martin, K. A. Rose, J. Salisbury, D. K. Steinberg, C. N. Trueman, R. W. Wilson, S. E. Wilson, Toward a better understanding of fish-based contribution to ocean carbon flux. *Limnol. Oceanogr.* **66**, 1639–1664 (2021).

54. P. Wassmann, K. N. Kosobokova, D. Slagstad, K. F. Drinkwater, R. R. Hopcroft, S. E. Moore, I. Ellingsen, R. J. Nelson, E. Carmack, E. Popova, J. Berge, The contiguous domains of Arctic Ocean advection: Trails of life and death. *Prog. Oceanogr.* **139**, 42–65 (2015).

55. B. A. Bluhm, K. N. Kosobokova, E. C. Carmack, A tale of two basins: An integrated physical and biological perspective of the deep Arctic Ocean. *Prog. Oceanogr.* **139**, 89–121 (2015).

56. A. Kraft, M. Graeve, D. Janssen, M. Greenacre, S. Falk-Petersen, Arctic pelagic amphipods: Lipid dynamics and life strategy. *J. Plankton Res.* **37**, 790–807 (2015).

57. S. Kaartvedt, Photoperiod may constrain the effect of global warming in arctic marine systems. *J. Plankton Res.* **30**, 1203–1206 (2008).

58. G. Johnsen, M. Candeloro, J. Berge, M. Moline, Glowing in the dark: Discriminating patterns of bioluminescence from different taxa during the Arctic polar night. *Polar Biol.* **37**, 707–713 (2014).

59. T.-Y. Chen, M. Frank, B. A. Haley, M. Gutjahr, R. F. Spielhagen, Variations of North Atlantic inflow to the Central Arctic Ocean over the last 14 million years inferred from hafnium and neodymium isotopes. *Earth Planet. Sci. Lett.* **353**, 82–92 (2012).

60. I. V. Polyakov, A. V. Pnyushkov, M. B. Alkire, I. M. Ashik, T. M. Baumann, E. C. Carmack, I. Goszczko, J. Guthrie, V. V. Ivanov, T. Kanzow, R. Krishfield, R. Kwok, A. Sundfjord, J. Morison, R. Rember, A. Yulin, Greater role for Atlantic inflows on sea-ice loss in the Eurasian Basin of the Arctic Ocean. *Science* **356**, 285–291 (2017).

61. I. V. Polyakov, M. B. Alkire, B. A. Bluhm, K. A. Brown, E. C. Carmack, M. Chierici, S. L. Danielson, I. Ellingsen, E. A. Ershova, K. Gårdfeldt, R. B. Ingvaldsen, A. V. Pnyushkov, D. Slagstad, P. Wassmann, Borealization of the Arctic Ocean in response to anomalous advection from sub-Arctic seas. *Front. Mar. Sci.* **7**, 491 (2020).

62. K. M. Lewis, G. L. van Dijken, K. R. Arrigo, Changes in phytoplankton concentration now drive increased Arctic Ocean primary production. *Science* **369**, 198–202 (2020).

63. I. Wiedmann, E. Ershova, B. A. Bluhm, E. M. Nöthig, R. R. Gradinger, K. Kosobokova, A. Boetius, What feeds the benthos in the Arctic basins? Assembling a carbon budget for the deep Arctic Ocean. *Front. Mar. Sci.* **7**, 224 (2020).

64. E. M. Nöthig, S. Ramonden, A. Haas, L. Hehemann, A. Walter, A. Bracher, C. Lalande, K. Metfies, I. Peeken, A. Bauerfeind, A. Boetius, Summertime chlorophyll *a* and particulate organic carbon standing stocks in surface waters of the Fram Strait and the Arctic Ocean (1991–2015). *Front. Mar. Sci.* **7**, 350 (2020).

65. D. Slagstad, F. J. Wassmann, I. Ellingsen, Physical constrains and productivity in the future Arctic Ocean. *Front. Mar. Sci.* **2**, 85 (2015).

66. D. A. Demer, L. Berger, M Bernasconi, E. Bethke, K. Boswell, D. Chu, R. Domokos, A. Dunford, S. Fässler, S. Gauthier, L. T. Hufnagle, J. M. Jech, N. Bouffant, A. Lebourges-Dhaussy, X. Lurton, G. J. Macaulay, Y. Perrot, T. Ryan, S. Parker-Stetter, S. Stienessen, T. Weber, N. Williamson, Calibration of acoustic instruments (ICES Cooperative Research Report 326, International Council for the Exploration of the Sea, 2015), 132 pp.

67. J. Stenvik, M. S. Wesmajervi, B. Damsgard, M. Delghandi, Genotyping of pantophysin I (Pan I) of Atlantic cod (*Gadus morhua* L.) by allele-specific PCR. *Mol. Ecol. Notes* **6**, 272–275 (2006).

68. G. H. Pogson, Nucleotide polymorphism and natural selection at the pantophysin (Pan I) locus in the Atlantic cod, *Gadus morhua* (L.). *Genetics* **157**, 317–330 (2001).

69. H. Høie, E. Otterlei, A. Folkvord, Temperature-dependent fractionation of stable oxygen isotopes in otoliths of juvenile cod (*Gadus morhua* L.). *ICES J. Mar. Sci.* **61**, 243–251 (2004).

70. M. Jakobsson, L. Mayer, B. Coakley, J. A. Dowdeswell, S. Forbes, B. Fridman, H. Hodnesdal, R. Noormets, R. Pedersen, M. Rebesco, H. W. Schenke, Y. Zarayskaya, D. Accettella, A. Armstrong, R. M. Anderson, P. Bienhoff, A. Camerlenghi, I. Church, M. Edwards, J. V. Gardner, J. K. Hall, B. Hell, O. Hestvik, Y. Kristoffersen, C. Marcussen, R. Mohammad, D. Mosher, S. V. Nghiem, M. T. Pedrosa, P. G. Travaglini, P. Weatherall, The International Bathymetric Chart of the Arctic Ocean (IBCAO) version 3.0. *Geophys. Res. Lett.* **39**, L12609 (2012).

according to the IACUC guidelines was necessary because the 15 fish were collected in waters not under the jurisdiction of any particular country. **Data and materials availability:** All data needed to evaluate the conclusions in this paper are present in the paper and/or the Supplementary Materials. All raw data (hydroacoustics, video recordings and CTD data) are stored in the MOSAiC Central Storage (MCS) at the Alfred Wegener Institute (AWI), Germany, and will be publicly available after 1 January 2023 following the MOSAiC data policy. The hydroacoustic raw data are also published in the Pangaea data repository at https://doi.

pangaea.de/10.1594/PANGAEA.916105; https://doi.pangaea.de/10.1594/PANGAEA.920008; and https://doi.pangaea.de/10.1594/PANGAEA.923587.

Science Advances

Unexpected fish and squid in the central Arctic deep scattering layer

Pauline Snoeijs-LeijonmalmHauke FloresSerdar SakinanNicole HildebrandtAnders SvensonGiulia CastellaniKim VaneFelix C. MarkCéline HeuzéSandra TippenhauerBarbara NiehoffJoakim HjelmJonas Hentati SundbergFokje L. SchaafsmaRonny Engelmann

View the article online
https://www.science.org/doi/10.1126/sciadv.abj7536
Permissions
https://www.science.org/help/reprints-and-permissions

Use of this article is subject to the Terms of service